

Double parton scattering in $\bar{p}p$ collisions at $\sqrt{s}=1.8$ TeV

F. Abe,¹⁷ H. Akimoto,³⁶ A. Akopian,³¹ M. G. Albrow,⁷ S. R. Amendolia,²⁷ D. Amidei,²⁰ J. Antos,³³ S. Aota,³⁶ G. Apollinari,³¹ T. Asakawa,³⁶ W. Ashmanskas,¹⁸ M. Atac,⁷ F. Azfar,²⁶ P. Azzi-Bacchetta,²⁵ N. Bacchetta,²⁵ W. Badgett,²⁰ S. Bagdasarov,³¹ M. W. Bailey,²² J. Bao,³⁹ P. de Barbaro,³⁰ A. Barbaro-Galtieri,¹⁸ V. E. Barnes,²⁹ B. A. Barnett,¹⁵ M. Barone,⁹ E. Barzi,⁹ G. Bauer,¹⁹ T. Baumann,¹¹ F. Bedeschi,²⁷ S. Behrends,³ S. Belforte,²⁷ G. Bellettini,²⁷ J. Bellinger,³⁸ D. Benjamin,³⁵ J. Benlloch,¹⁹ J. Bensinger,³ D. Benton,²⁶ A. Beretvas,⁷ J. P. Berge,⁷ J. Berryhill,⁵ S. Bertolucci,⁹ B. Bevensee,²⁶ A. Bhatti,³¹ K. Biery,⁷ M. Binkley,⁷ D. Bisello,²⁵ R. E. Blair,¹ C. Blocker,³ A. Bodek,³⁰ W. Bokhari,¹⁹ V. Bolognesi,² G. Bolla,²⁹ D. Bortoletto,²⁹ J. Boudreau,²⁸ L. Breccia,² C. Bromberg,²¹ N. Bruner,²² E. Buckley-Geer,⁷ H. S. Budd,³⁰ K. Burkett,²⁰ G. Busetto,²⁵ A. Byon-Wagner,⁷ K. L. Byrum,¹ J. Cammerata,¹⁵ C. Campagnari,⁷ M. Campbell,²⁰ A. Caner,²⁷ W. Carithers,¹⁸ D. Carlsmith,³⁸ A. Castro,²⁵ D. Cauz,²⁷ Y. Cen,³⁰ F. Cervelli,²⁷ P. S. Chang,³³ P. T. Chang,³³ H. Y. Chao,³³ J. Chapman,²⁰ M.-T. Cheng,³³ G. Chiarelli,²⁷ T. Chikamatsu,³⁶ C. N. Chiu,³³ L. Christofek,¹³ S. Cihangir,⁷ A. G. Clark,¹⁰ M. Cobal,²⁷ E. Cocca,²⁷ M. Contreras,⁵ J. Conway,³² J. Cooper,⁷ M. Cordelli,⁹ C. Couyoumtzelis,¹⁰ D. Crane,¹ D. Cronin-Hennessy,⁶ R. Culbertson,⁵ T. Daniels,¹⁹ F. DeJongh,⁷ S. Delchamps,⁷ S. Dell'Agnello,²⁷ M. Dell'Orso,²⁷ R. Demina,⁷ L. Demortier,³¹ M. Deninno,² P. F. Derwent,⁷ T. Devlin,³² J. R. Dittmann,⁶ S. Donati,²⁷ J. Done,³⁴ T. Dorigo,²⁵ A. Dunn,²⁰ N. Eddy,²⁰ K. Einsweiler,¹⁸ J. E. Elias,⁷ R. Ely,¹⁸ E. Engels, Jr.,²⁸ D. Errede,¹³ S. Errede,¹³ Q. Fan,³⁰ G. Feild,³⁹ C. Ferretti,²⁷ I. Fiori,² B. Flaughner,⁷ G. W. Foster,⁷ M. Franklin,¹¹ M. Frautschi,³⁵ J. Freeman,⁷ J. Friedman,¹⁹ H. Frisch,⁵ Y. Fukui,¹⁷ S. Funaki,³⁶ S. Galeotti,²⁷ M. Gallinaro,²⁶ O. Ganel,³⁵ M. Garcia-Sciveres,¹⁸ A. F. Garfinkel,²⁹ C. Gay,¹¹ S. Geer,⁷ D. W. Gerdes,¹⁵ P. Giannetti,²⁷ N. Giokaris,³¹ P. Giromini,⁹ G. Giusti,²⁷ L. Gladney,²⁶ D. Glenzinski,¹⁵ M. Gold,²² J. Gonzalez,²⁶ A. Gordon,¹¹ A. T. Goshaw,⁶ Y. Gotra,²⁵ K. Goulianos,³¹ H. Grassmann,²⁷ L. Groer,³² C. Grosso-Pilcher,⁵ G. Guillian,²⁰ R. S. Guo,³³ C. Haber,¹⁸ E. Hafen,¹⁹ S. R. Hahn,⁷ R. Hamilton,¹¹ R. Handler,³⁸ R. M. Hans,³⁹ F. Happacher,⁹ K. Hara,³⁶ A. D. Hardman,²⁹ B. Harral,²⁶ R. M. Harris,⁷ S. A. Hauger,⁶ J. Hauser,⁴ C. Hawk,³² E. Hayashi,³⁶ J. Heinrich,²⁶ B. Hinrichsen,¹⁴ K. D. Hoffman,²⁹ M. Hohlmann,⁵ C. Holck,²⁶ R. Hollebeek,²⁶ L. Holloway,¹³ S. Hong,²⁰ G. Houk,²⁶ P. Hu,²⁸ B. T. Huffman,²⁸ R. Hughes,²³ J. Huston,²¹ J. Huth,¹¹ J. Hylen,⁷ H. Ikeda,³⁶ M. Incagli,²⁷ J. Incandela,⁷ G. Introzzi,²⁷ J. Iwai,³⁶ Y. Iwata,¹² H. Jensen,⁷ U. Joshi,⁷ R. W. Kadel,¹⁸ E. Kajfasz,²⁵ H. Kambara,¹⁰ T. Kamon,³⁶ T. Kaneko,³⁶ K. Karr,³⁷ H. Kasha,³⁹ Y. Kato,²⁴ T. A. Keaffaber,²⁹ K. Kelley,¹⁹ R. D. Kennedy,⁷ R. Kephart,⁷ P. Kesten,¹⁸ D. Kestenbaum,¹¹ H. Keutelian,⁷ F. Keyvan,⁴ B. Kharadia,¹³ B. J. Kim,³⁰ D. H. Kim,^{7,*} H. S. Kim,¹⁴ S. B. Kim,²⁰ S. H. Kim,³⁶ Y. K. Kim,¹⁸ L. Kirsch,³ P. Koehn,²³ K. Kondo,³⁶ J. Konigsberg,⁸ S. Kopp,⁵ K. Kordas,¹⁴ A. Korytov,⁸ W. Koska,⁷ E. Kovacs,^{7,*} W. Kowald,⁶ M. Krasberg,²⁰ J. Kroll,⁷ M. Kruse,³⁰ T. Kuwabara,³⁶ S. E. Kuhlmann,¹ E. Kuns,³² A. T. Laasanen,²⁹ S. Lami,²⁷ S. Lammel,⁷ J. I. Lamoureux,³ M. Lancaster,¹⁸ T. LeCompte,¹ S. Leone,²⁷ J. D. Lewis,⁷ P. Limon,⁷ M. Lindgren,⁴ T. M. Liss,¹³ J. B. Liu,³⁰ Y. C. Liu,³³ N. Lockyer,²⁶ O. Long,²⁶ C. Loomis,³² M. Loreti,²⁵ J. Lu,³⁴ D. Lucchesi,²⁷ P. Lukens,⁷ S. Lusin,³⁸ J. Lys,¹⁸ K. Maeshima,⁷ A. Maghakian,³¹ P. Maksimovic,¹⁹ M. Mangano,²⁷ J. Mansour,²¹ M. Mariotti,²⁵ J. P. Marriner,⁷ A. Martin,³⁹ J. A. J. Matthews,²² R. Mattingly,¹⁹ P. McIntyre,³⁴ P. Melese,³¹ A. Menzione,²⁷ E. Meschi,²⁷ S. Metzler,²⁶ C. Miao,²⁰ T. Miao,⁷ G. Michail,¹¹ R. Miller,²¹ H. Minato,³⁶ S. Miscetti,⁹ M. Mishina,¹⁷ H. Mitsushio,³⁶ T. Miyamoto,³⁶ S. Miyashita,³⁶ N. Moggi,²⁷ Y. Morita,¹⁷ A. Mukherjee,⁷ T. Muller,¹⁶ P. Murat,²⁷ H. Nakada,³⁶ I. Nakano,³⁶ C. Nelson,⁷ D. Neuberger,¹⁶ C. Newman-Holmes,⁷ C.-Y. P. Ngan,¹⁹ M. Ninomiya,³⁶ L. Nodulman,¹ S. H. Oh,⁶ K. E. Ohl,³⁹ T. Ohmoto,¹² T. Ohsugi,¹² R. Oishi,³⁶ M. Okabe,³⁶ T. Okusawa,²⁴ R. Oliveira,²⁶ J. Olsen,³⁸ C. Pagliarone,²⁷ R. Paoletti,²⁷ V. Papadimitriou,³⁵ S. P. Pappas,³⁹ N. Parashar,²⁷ S. Park,⁷ A. Parri,⁹ J. Patrick,⁷ G. Pauletta,²⁷ M. Paulini,¹⁸ A. Perazzo,²⁷ L. Pescara,²⁵ M. D. Peters,¹⁸ T. J. Phillips,⁶ G. Piacentino,²⁷ M. Pillai,³⁰ K. T. Pitts,⁷ R. Plunkett,⁷ L. Pondrom,³⁸ J. Proudfoot,¹ F. Ptohos,¹¹ G. Punzi,²⁷ K. Ragan,¹⁴ D. Reher,¹⁸ A. Ribon,²⁵ F. Rimondi,² L. Ristori,²⁷ W. J. Robertson,⁶ T. Rodrigo,²⁷ S. Rolli,³⁷ J. Romano,⁵ L. Rosenson,¹⁹ R. Roser,¹³ T. Saab,¹⁴ W. K. Sakumoto,³⁰ D. Saltzberg,⁵ A. Sansoni,⁹ L. Santi,²⁷ H. Sato,³⁶ P. Schlabach,⁷ E. E. Schmidt,⁷ M. P. Schmidt,³⁹ A. Scribano,²⁷ S. Segler,⁷ S. Seidel,²² Y. Seiya,³⁶ G. Sganos,¹⁴ M. D. Shapiro,¹⁸ N. M. Shaw,²⁹ Q. Shen,²⁹ P. F. Shepard,²⁸ M. Shimojima,³⁶ M. Shochet,⁵ J. Siegrist,¹⁸ A. Sill,³⁵ P. Sinervo,¹⁴ P. Singh,²⁸ J. Skarha,¹⁵ K. Sliwa,³⁷ F. D. Snider,¹⁵ T. Song,²⁰ J. Spalding,⁷ T. Speer,¹⁰ P. Sphicas,¹⁹ F. Spinella,²⁷ M. Spiropulu,¹¹ L. Spiegel,⁷ L. Stanco,²⁵ J. Steele,³⁸ A. Stefanini,²⁷ K. Strahl,¹⁴ J. Strait,⁷ R. Ströhmer,^{7,*} D. Stuart,⁷ G. Sullivan,⁵ K. Sumorok,¹⁹ J. Suzuki,³⁶ T. Takada,³⁶ T. Takahashi,²⁴ T. Takano,³⁶ K. Takikawa,³⁶ N. Tamara,¹² B. Tannenbaum,²² F. Tartarelli,²⁷ W. Taylor,¹⁴ P. K. Teng,³³ Y. Teramoto,²⁴ S. Tether,¹⁹ D. Theriot,⁷ T. L. Thomas,²² R. Thun,²⁰ R. Thurman-Keup,¹ M. Timko,³⁷ P. Tipton,³⁰ A. Titov,³¹ S. Tkaczyk,⁷ D. Toback,⁵ K. Tollefson,³⁰ A. Tollestrup,⁷ H. Toyoda,²⁴ W. Trischuk,¹⁴ J. F. de Troconiz,¹¹ S. Truitt,²⁰ J. Tseng,¹⁹ N. Turini,²⁷ T. Uchida,³⁶ N. Uemura,³⁶ F. Ukegawa,²⁶ G. Unal,²⁶ J. Valls,^{7,*} S. C. van den Brink,²⁸ S. Vejcek III,²⁰ G. Velev,²⁷ R. Vidal,⁷ R. Vilar,^{7,*} M. Vondracek,¹³ D. Vucinic,¹⁹ R. G. Wagner,¹ R. L. Wagner,⁷ J. Wahl,⁵ N. B. Wallace,²⁷ A. M. Walsh,³² C. Wang,⁶ C. H. Wang,³³ J. Wang,⁵ M. J. Wang,³³ Q. F. Wang,³¹ A. Warburton,¹⁴ T. Watts,³² R. Webb,³⁴ C. Wei,⁶ H. Wenzel,¹⁶ W. C. Wester III,⁷ A. B. Wicklund,¹ E. Wicklund,⁷ R. Wilkinson,²⁶ H. H. Williams,²⁶ P. Wilson,⁵ B. L. Winer,²³ D. Winn,²⁰ D. Wolinski,²⁰ J. Wolinski,²¹ S. Worm,²² X. Wu,¹⁰ J. Wyss,²⁵ A. Yagil,⁷ W. Yao,¹⁸ K. Yasuoka,³⁶ Y. Ye,¹⁴ G. P. Yeh,⁷ P. Yeh,³³ M. Yin,⁶ J. Yoh,⁷ C. Yosef,²¹ T. Yoshida,²⁴ D. Yovanovitch,⁷ I. Yu,⁷ L. Yu,²² J. C. Yun,⁷ A. Zanetti,²⁷ F. Zetti,²⁷ L. Zhang,³⁸ W. Zhang,²⁶ and S. Zucchelli²

(CDF Collaboration)

- ¹Argonne National Laboratory, Argonne, Illinois 60439
²Istituto Nazionale di Fisica Nucleare, University of Bologna, I-40127 Bologna, Italy
³Brandeis University, Waltham, Massachusetts 02264
⁴University of California at Los Angeles, Los Angeles, California 90024
⁵University of Chicago, Chicago, Illinois 60638
⁶Duke University, Durham, North Carolina 28708
⁷Fermi National Accelerator Laboratory, Batavia, Illinois 60510
⁸University of Florida, Gainesville, Florida 33611
⁹Laboratori Nazionali di Frascati, Istituto Nazionale di Fisica Nucleare, I-00044 Frascati, Italy
¹⁰University of Geneva, CH-1211 Geneva 4, Switzerland
¹¹Harvard University, Cambridge, Massachusetts 02138
¹²Hiroshima University, Higashi-Hiroshima 724, Japan
¹³University of Illinois, Urbana, Illinois 61801
¹⁴Institute of Particle Physics, McGill University, Montreal H3A 2T8,
and University of Toronto, Toronto, Canada M5S 1A7
¹⁵The Johns Hopkins University, Baltimore, Maryland 21218
¹⁶Universität Karlsruhe, 76128 Karlsruhe, Germany
¹⁷National Laboratory for High Energy Physics (KEK), Tsukuba, Ibaraki 315, Japan
¹⁸Ernest Orlando Lawrence Berkeley National Laboratory, Berkeley, California 94720
¹⁹Massachusetts Institute of Technology, Cambridge, Massachusetts 02139
²⁰University of Michigan, Ann Arbor, Michigan 48109
²¹Michigan State University, East Lansing, Michigan 48824
²²University of New Mexico, Albuquerque, New Mexico 87132
²³The Ohio State University, Columbus, Ohio 43220
²⁴Osaka City University, Osaka 588, Japan
²⁵Università di Padova, Istituto Nazionale di Fisica Nucleare, Sezione di Padova, I-36132 Padova, Italy
²⁶University of Pennsylvania, Philadelphia, Pennsylvania 19104
²⁷Istituto Nazionale di Fisica Nucleare, University and Scuola Normale Superiore of Pisa, I-56100 Pisa, Italy
²⁸University of Pittsburgh, Pittsburgh, Pennsylvania 15270
²⁹Purdue University, West Lafayette, Indiana 47907
³⁰University of Rochester, Rochester, New York 14628
³¹Rockefeller University, New York, New York 10021
³²Rutgers University, Piscataway, New Jersey 08854
³³Academia Sinica, Taipei, Taiwan 11530, Republic of China
³⁴Texas A&M University, College Station, Texas 77843
³⁵Texas Tech University, Lubbock, Texas 79409
³⁶University of Tsukuba, Tsukuba, Ibaraki 315, Japan
³⁷Tufts University, Medford, Massachusetts 02155
³⁸University of Wisconsin, Madison, Wisconsin 53806
³⁹Yale University, New Haven, Connecticut 06511

(Received 14 April 1997)

A strong signal for double parton (DP) scattering is observed in a 16 pb^{-1} sample of $\bar{p}p \rightarrow \gamma/\pi^0 + 3 \text{ jets} + X$ data from the CDF experiment at the Fermilab Tevatron. In DP events, two separate hard scatterings take place in a single $\bar{p}p$ collision. We isolate a large sample of data ($\sim 14\,000$ events) of which 53% are found to be DP. The process-independent parameter of double parton scattering, σ_{eff} , is obtained without reference to theoretical calculations by comparing observed DP events to events with hard scatterings in separate $\bar{p}p$ collisions. The result $\sigma_{\text{eff}} = (14.5 \pm 1.7^{+1.7}_{-2.3}) \text{ mb}$ represents a significant improvement over previous measurements, and is used to constrain simple models of parton spatial density. The Feynman x dependence of σ_{eff} is investigated and none is apparent. Further, no evidence is found for kinematic correlations between the two scatterings in DP events. [S0556-2821(97)01619-6]

PACS number(s): 13.87.Ce, 12.38.Qk, 13.85.Ni, 14.20.Dh

I. INTRODUCTION

Traditionally, studies of proton structure at $\bar{p}p$ colliders have focused on the kinematics of individual parton constitu-

ents, e.g., on the character and evolution of the structure functions. New and complementary information on the structure of the proton can be obtained by identifying and analyzing events in which two parton-parton hard scatterings take place within one $\bar{p}p$ collision. This process, double parton scattering [1], provides information on both the spatial distribution of partons within the proton, and on possible

*Visitor.

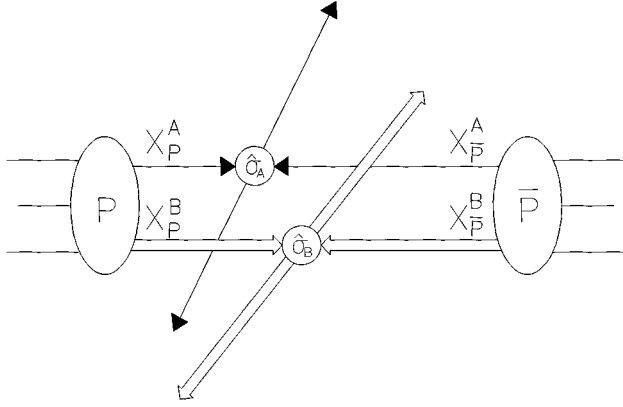


FIG. 1. Schematic diagram of double parton scattering in $\bar{p}p$ collisions. Two pairs of partons undergo hard scatterings; the scatterings are labeled A and B , and the Feynman x 's of the four initial state partons are labeled by the baryon from which they originate and the scattering to which they contribute.

parton-parton correlations, topics difficult to address within the framework of perturbative QCD. Both the absolute rate for the double parton (DP) process, and any dynamics that correlations may introduce, are therefore of interest. Furthermore, an understanding of DP is important for estimating backgrounds to such processes as diboson (W^+W^- , etc.) and boson + jets production, and for making accurate predictions of hard-scattering rates at future high energy hadron colliders such as the CERN Large Hadron Collider (LHC).

A DP scattering occurring within a $\bar{p}p$ collision is illustrated schematically in Fig. 1. In the simplest model, DP produces a final state that mimics a combination of two independent scatterings. It is customary [2–5] to express the cross section for this process as the product of the cross sections for the individual hard scatterings divided by a scaling factor, σ_{eff} , with units of area. For the DP process comprised of scatterings A and B ,

$$\sigma_{\text{DP}} \equiv m \frac{\sigma_A \sigma_B}{2\sigma_{\text{eff}}}. \quad (1)$$

The factor of one-half, also customary, incorporates the assumption that the number of parton-parton interactions per collision is distributed according to Poisson statistics [6]. The m factor has the value $m=2$ when A and B are distinguishable scatterings, and $m=1$ when they are indistinguishable [7].

The process-independent parameter σ_{eff} contains the information on the spatial distribution of partons [8]. In Eq. (1), $\sigma_B/(2\sigma_{\text{eff}})$ is the probability of hard scattering B taking place given A , and this will be larger or smaller depending on the parton spatial density. If the parton density were “clumpy,” with partons concentrated within small regions inside the proton, B would be more likely to occur given A , because the A scattering preselects $\bar{p}p$ collisions in which “clumps” have overlapped. By contrast, a uniform parton density throughout the proton would produce a larger σ_{eff} and a smaller σ_{DP} , since apart from trivial geometric effects (Sec. IX A) the presence of A would not increase the probability of B . Based on this simple “solid sphere” model of

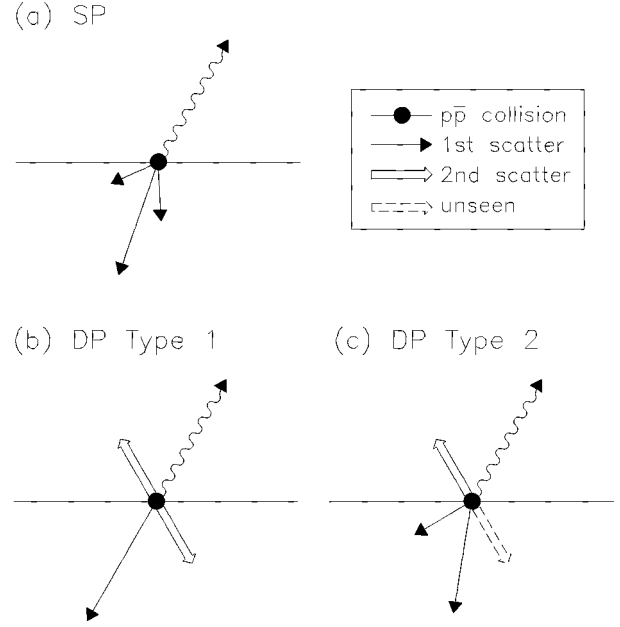


FIG. 2. Schematic diagrams of the photon + 3 jet final state produced in a single $\bar{p}p$ collision. (a) SP production, in which a single hard scattering takes place. (b) DP consisting of photon + 1 jet production overlaid with dijet production. (c) DP consisting of photon + 2 jet production overlaid with dijet production, where one of the two jets of the dijet is not seen in the detector.

proton structure, and the measured inelastic $\bar{p}p$ cross section at $\sqrt{s}=1.8$ TeV [9], the expected value for σ_{eff} is ≈ 11 mb.

Previous measurements of σ_{eff} have come from the AFS, UA2, and Collider Detector at Fermilab (CDF) experiments. Each experiment searched a four-jet data sample, for which the DP signature is an uncorrelated pair of two-jet systems (two dijets) in the final state. For these measurements the m factor in Eq. (1) is unity. The CDF analysis of Ref. [5], using jets with momentum transverse to the beam direction (p_T) above 25 GeV/ c , found evidence for DP scattering at the level of $5.4^{+1.6}_{-2.0}\%$ of the events. The value extracted for σ_{eff} was $12.1^{+10.7}_{-5.4}$ mb. The AFS experiment measured $\sigma_{\text{eff}} \sim 5$ mb [3], while UA2 chose to place a lower limit of $\sigma_{\text{eff}} > 8.3$ mb at 95% C.L. [4].

This paper documents a measurement of the DP process from the Collider Detector at Fermilab (CDF). A summary of this extensive analysis is given in Ref. [10]. The final state studied is photon + 3 jets (+X). From this point on, unless specifically stated otherwise, “photon” is taken to mean either a single direct photon (γ), or multiple photons from neutral meson decay in jet fragmentation which approximately mimic a single photon (π^0). In this final state, the DP process is comprised of a photon-jet scattering and a dijet scattering. This leads to two observable configurations yielding a photon + 3 jets: a photon + 1 jet system overlaid with both jets from the dijet, or a photon + 2 jets system (one jet from gluon bremsstrahlung) plus one observed jet from the dijet. These two types of DP events are illustrated in Fig. 2. The single parton-parton (SP) scattering background is photon-jet production with bremsstrahlung radiation of two gluons. Compared to the previous CDF analysis, the photon + 3 jet dataset has two advantages: (1) the jets are accepted down to low energies where the cross section for the dijet

scattering in DP is large; and (2) the better energy measurement of photons at CDF (relative to jets) aids in distinguishing DP from SP. In consequence, the present analysis benefits from a substantial DP event sample and an order of magnitude improvement in the ratio of DP to SP events over the earlier CDF study. These improvements have permitted an investigation of the kinematic dependence of σ_{eff} and a search for correlations between the two scatterings. Additionally, a new technique for extracting σ_{eff} has been developed, which is independent of theoretical input and its uncertainties.

The structure of this paper is as follows. The method for obtaining σ_{eff} is outlined in Sec. II. The data sample and models for signals and backgrounds are described in Secs. III and IV. Distinguishing kinematic variables are discussed in Sec. V. In Secs. VI and VII we determine the numbers of double parton events and multiple collision “pile-up” events in our data sample, and use these in Sec. VIII to derive σ_{eff} . In Sec. IX the measured value of σ_{eff} is used to constrain simple models of parton spatial density, and searches for possible Feynman x dependence of σ_{eff} and kinematic correlations between the two scatterings are conducted. Lastly, a series of appendices describe the following aspects of the analysis in detail: the properties of low energy jets at CDF (Appendix A), higher order backgrounds to DP (Appendix B), and additional details on the σ_{eff} extraction technique (Appendix C).

II. METHOD FOR EXTRACTING σ_{eff}

In previous analyses σ_{eff} has been derived from measured DP cross sections, using QCD calculations of the two cross sections in Eq. (1). Theoretical calculations of dijet and photon production suffer from sizable uncertainties [11,12]. In the present analysis, σ_{eff} is extracted independently of theory, through a comparison of the number of observed DP events to the number of events with hard scatterings at two separate $\bar{p}p$ collisions within the same beam crossing. This latter class of events will be referred to as double interactions (DI’s). Because this method does not rely on theoretical input, it represents a substantial advance over previous measurements.

The DI process, with a photon + 1 or 2 jets at one collision, and 1 or 2 jets at another, is shown schematically in Figs. 3(b) and 3(c). Note that not all events with two collisions, such as the event shown in Fig. 3(a), are considered DI’s, only those with hard scatterings at both collisions. DI events should be kinematically identical to DP events if scatterings in the DP process are uncorrelated.

We now relate DP and DI production. Given a beam crossing with two non-single-diffractive (NSD) inelastic $\bar{p}p$ collisions, the probability for a DI in that crossing is

$$\text{Probability for DI} = 2 \left(\frac{\sigma_{\gamma/\pi^0}}{\sigma_{\text{NSD}}} \right) \left(\frac{\sigma_J}{\sigma_{\text{NSD}}} \right). \quad (2)$$

In symbolic fashion, we write σ_{γ/π^0} and σ_J as the cross sections for producing γ/π^0 + 1 or 2 jets, and 1 or 2 jets, respectively, which taken together yield γ/π^0 + 3 jet events. These cross sections do not need to be specified in more detail (see below). The cross section for NSD $\bar{p}p$ interactions

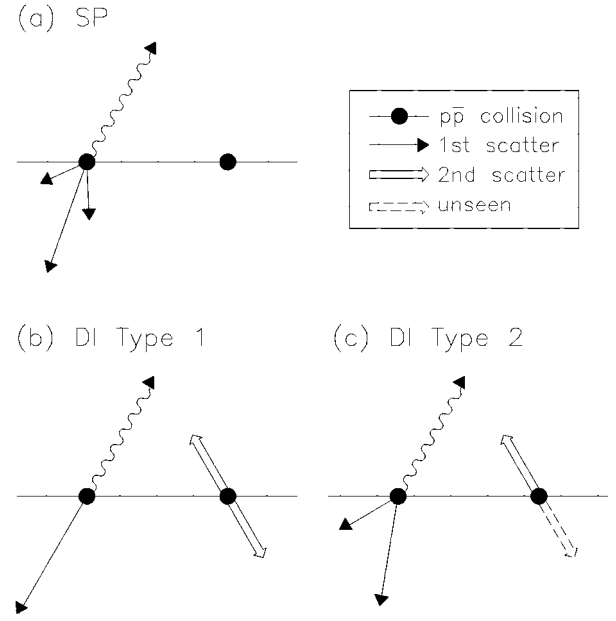


FIG. 3. Schematic diagrams of the photon + 3 jet final state produced in events with two $\bar{p}p$ collisions. (a) SP production at one collision together with an inelastic (soft) second collision. (b) DI production consisting of a photon + 1 jet scattering from one collision overlaid with a dijet from the second. (c) DI production consisting of a photon + 2 jet scattering from one collision overlaid with a dijet from the second, where one of the two jets of the dijet is not seen in the detector.

is written σ_{NSD} . The factor of 2 is combinatorial: the photon and jet scatterings can be ordered in two ways with respect to the two collisions. The number of DI events, to first order, is this probability multiplied by the number of beam crossings with 2 NSD collisions, $N_c(2)$:

$$N_{\text{DI}} = 2 \left(\frac{\sigma_{\gamma/\pi^0}}{\sigma_{\text{NSD}}} \right) \left(\frac{\sigma_J}{\sigma_{\text{NSD}}} \right) N_c(2). \quad (3)$$

Following the same line of argument, we predict the number of DP events. For the purposes of this derivation we assume that DP events have one collision per beam crossing. In Appendix C, we demonstrate that the m factor in Eq. (1) is 2 for the photon + 3 jet final state used in this analysis. Thus, given a beam crossing with one NSD collision, the probability for DP and the number of DP events are to first order

$$\text{Probability for DP} = \frac{\sigma_{\text{DP}}}{\sigma_{\text{NSD}}} = \frac{\sigma_{\gamma/\pi^0} \sigma_J}{\sigma_{\text{eff}} \sigma_{\text{NSD}}}, \quad (4)$$

$$N_{\text{DP}} = \left(\frac{\sigma_{\gamma/\pi^0} \sigma_J}{\sigma_{\text{eff}} \sigma_{\text{NSD}}} \right) N_c(1), \quad (5)$$

where $N_c(1)$ is the number of beam crossings with a single NSD $\bar{p}p$ collision. We take the ratio of Eqs. (3) and (5) and solve for σ_{eff} :

$$\sigma_{\text{eff}} = \left(\frac{N_{\text{DI}}}{N_{\text{DP}}} \right) \left(\frac{N_c(1)}{2N_c(2)} \right) \sigma_{\text{NSD}}. \quad (6)$$

In the above, σ_{γ/π^0} and σ_J , the cross sections which are uncertain theoretically, have cancelled. Of the remaining parameters, σ_{NSD} is known [9], and the numbers of events N_{DP} and N_{DI} will be measured. The number of beam crossings with n NSD collisions, $N_c(n)$, is calculable: for a given amount of data taken at some instantaneous Tevatron luminosity, $N_c(n)$ is a Poisson distribution in n , with mean n given by σ_{NSD} , the instantaneous luminosity, and the Tevatron beam crossing frequency. Modifications to Eq. (6) resulting from the efficiency for identifying collisions and event acceptance are discussed in Sec. VIII and Appendix C.

III. DATA SAMPLES

Data were taken with the CDF detector, which is described in detail elsewhere [13]. We outline here the detector components important for this analysis. The location of the collision vertex (or vertices) along the beam line is established with a set of time projection chambers (VTX) around the beam pipe. The momenta of charged particles are reconstructed in the central tracking chamber (CTC), a cylindrical drift chamber immersed in a 1.4 T axial magnetic field. Photons are detected in the central calorimeter which spans 2π in ϕ and ± 1.1 in pseudorapidity η . Projective towers in the calorimeter are divided into electromagnetic (EM) and hadronic (HAD) compartments. A strip chamber (CES) embedded in the EM calorimeter near shower maximum measures transverse shower profiles. A set of preradiator chambers (CPR) located in front of the central calorimeter counts photon conversions. The plug and forward calorimeters extend coverage for jet identification to $|\eta| < 4.2$. Instantaneous luminosity measurements are accomplished using a pair of up- and down-stream scintillator hodoscopes (BBC counters). The CDF coordinate system defines the z axis along the beam line, and the polar angle with respect to this axis is θ .

The data sample consists of an integrated luminosity of 16 pb^{-1} accumulated in the 1992–3 Collider Run. Average instantaneous luminosity for this running period was approximately $2.7 \times 10^{30} (\text{cm}^2 \text{ sec})^{-1}$. Data were taken with an inclusive photon trigger which required a transverse energy deposition [$E_T = E \sin(\theta)$] in the central calorimeter above 16 GeV, predominantly in the EM compartment, with transverse energy flow consistent with a photon shower [14]. The trigger also required less than 4 GeV of additional calorimeter E_T (EM+HAD) in a cone of $\Delta R < 0.7$ around the photon candidate ($\Delta R = \sqrt{\Delta\eta^2 + \Delta\phi^2}$). Off-line, photon candidates were required to have $|\eta| < 0.9$ to ensure good containment in the central calorimeter, and a correction for trigger inefficiency as a function of photon E_T was applied [15]. Accepted events include both single direct photons and merged multiple photons. A second trigger sample of interest is the minimum bias dataset, collected by requiring coincident signals in both sets of BBC counters.

No jets were required in the trigger. Off-line, jet reconstruction [16] was performed using a cone of radius 0.7 in (η, ϕ) to define jet E_T . Jet E_T 's were corrected for the response of the calorimeter as a function of η but not for energy losses (such as from calorimeter nonlinearity and uninstrumented regions). Events having three and only three jets with $E_T > 5 \text{ GeV}$, anywhere in the calorimeter, were ac-

cepted. In decreasing order of E_T , the transverse energies of the three jets are $E_T(1)$, $E_T(2)$, and $E_T(3)$. The photon and jets were required to be separated by $\Delta R > 0.8$, and pairs of jets by $\Delta R > 0.7$. A further requirement of $E_T < 7 \text{ GeV}$ was made on the two lowest E_T jets. This enhances DP over SP, since the E_T spectrum of the DP jets is softer than the SP background (Sec. VI).

The events were subdivided into double parton and double interaction candidate samples based on the number of observed $\bar{p}p$ collisions per crossing. The requirement for DP candidates was a single collision vertex found in the VTX, and the requirement for DI candidates was two VTX vertices. No additional VTX vertices were allowed. These candidate samples, passing all the selection criteria discussed above, are referred to as the 1VTX and 2VTX data sets. A total of 13 747 events in the 1VTX sample and 4904 events in the 2VTX sample pass all requirements. After the trigger efficiency correction the effective number of events is 16 853 and 5983. These numbers are reiterated in Table I, along with the uses to which the data sets will be put. (Additional data sets described in Secs. VI and VII are also summarized in Table I.)

The two least energetic jets in the 1VTX and 2VTX data sets have lower E_T than the jets of previously published CDF measurements [17]. As a result, the interpretation of these objects as products of hard scatterings must be justified; this we do in Appendix A. We find that 5 GeV jets are the result of real jet production, as opposed to instrumental effects. We note, however, that detector response is poor at such low E_T 's: for parton $E_T \sim 5 \text{ GeV}$, E_T losses amount to 20%, calorimeter resolution is 2 GeV and jet-finding efficiency is 30%. As a result, the relationship between the partonic and observed jet properties is complicated and uncertain. Also, at low energies, perturbative QCD calculations for jet cross sections may not be reliable. The virtue of this analysis is that the σ_{eff} measurement is independent of these concerns, since all comparisons to theoretical cross section calculations are avoided. The presence of observed $\gamma/\pi^0 + 3$ jet systems in DP and DI events in data is all that is required to obtain σ_{eff} .

IV. MODELS FOR SIGNAL AND BACKGROUND

To identify the presence of the DP process in our data, and to extract σ_{eff} , predictions are required for the properties of the DP and DI processes, and for the SP background to the 2VTX sample [Fig. 3(a)]. Models for these processes are described below, and their uses are summarized in Table I.

Models were obtained by combining pairs of CDF events. For the DP and DI models, referred to as MIXDP and MIXDI, CDF inclusive photon events were mixed with minimum bias events, with both sets of events required to have a single VTX vertex and ≥ 1 jet. The resulting mixed events, which by construction include at least one jet from each “ingredient event,” were required to pass the $\gamma/\pi^0 + 3$ jet event selection. The mixing process is illustrated in Fig. 4. We find that roughly 75% of these events have a single reconstructed jet, rather than a dijet, from the minimum bias ingredient event. The MIXDP and MIXDI models differ only in the size of the “underlying event” energy contribution to the jets and photon, which arises from soft interactions among spectator partons in the p and \bar{p} . Studies of the DP candidate sample

TABLE I. Summary of the data sets, selection criteria, and models for signal and background used in the identification of the double parton (DP) and double interaction (DI) processes. In all cases the $\gamma/\pi^0 + 3$ jet final state is modeled, with photon $E_T > 16$ GeV and jet $E_T > 5$ GeV. Unless indicated otherwise, jets are accepted within the full CDF calorimeter ($|\eta| < 4.2$). The search for DP (DI) is conducted in datasets and models with a single (two) observed $\bar{p}p$ vertex. The PYTHIA shower Monte Carlo program is used as a crosscheck only.

Process studied	Data sets and selection criteria	No. events in data	Model for signal	Model for background
DP, in 1 VTX vertex events	1VTX A set: $5 < E_T(2) < 7$ GeV	16853	MIXDP event mixing, ≥ 1 jet from each event.	PYTHIA shower MC, SP $\gamma/\pi^0 + 3$ jets.
	1VTX B set: $7 < E_T(2) < 9$ GeV	3727	Underlying event E_T from 1 $\bar{p}p$ collision.	Underlying event E_T from 1 $\bar{p}p$ collision.
	DP enriched: $5 < E_T(2) < 7$ GeV, $\Delta S < 1.2$	2575		
DI, in 2 VTX vertex events	2VTX: $5 < E_T(2) < 7$ GeV	5983	MIXDI event mixing, ≥ 1 jet from each event.	MIX2V event mixing, $\gamma/\pi^0 + 3$ jets from one event.
	Jet origin: $E_T(2) > 5$ GeV, $ \eta < 1.3$ for all jets, ≥ 1 CTC track per jet	1333	Underlying event E_T from $\bar{p}p$ collisions.	Underlying event E_T from 2 $\bar{p}p$ collisions.

indicate that a typical single collision underlying event is present in these events, whereas for DI events with two $\bar{p}p$ collisions approximately twice that level is seen [18]. This difference has an impact primarily on event acceptance (Sec. VIII). We note that, by construction, the DP model assumes independent scatterings.

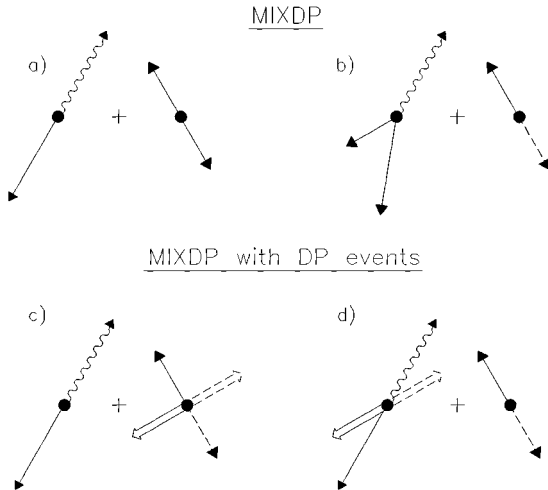


FIG. 4. Schematic diagram of MIXDP mixing. Four constructions of MIXDP events are shown. (a) A CDF photon + 1 jet event mixed with a CDF dijet event. (b) A photon + 2 jet event mixed with a dijet event where one of the two jets of the dijet is not seen in the detector. (c) A photon + 1 jet event mixed with a double-dijet DP event where one jet of each dijet is lost. (d) A DP event in the (photon+1 jet)+dijet final state with one jet from the dijet lost, mixed with a dijet event with one jet lost. Configurations (c) and (d) model triple parton scattering events.

The non-DI background in the 2VTX sample [Fig. 3(a)] consists of multiple collision events in which a $\gamma/\pi^0 + 3$ jets hard scattering is accompanied by a second $\bar{p}p$ collision without a hard scattering (specifically, with no jet above 5 GeV E_T). The model for this background, MIX2V, was obtained by mixing single vertex $\gamma/\pi^0 + 3$ jet events and minimum bias events without jets, again with an underlying event energy appropriate for events with two collisions.

These data-derived models alone are used to determine the numbers of DP and DI events in data. As a cross check, however, a prediction for the SP background to the 1VTX dataset [Fig. 2(a)] was obtained from the PYTHIA Monte Carlo program [19]. To ensure that both the γ and π^0 events in our data were modeled, PYTHIA Version 5.702 was used to generate all $2 \rightarrow 2$ partonic processes, with structure function CTEQ2M ($\mu^2 = p_T^2$). Multiple parton scatterings within the $\bar{p}p$ collision were disabled. Event generation was followed by detector simulation [20], event reconstruction, and event selection.

V. DISTINGUISHING VARIABLES

To differentiate between the DP and SP processes in data, we exploit the independence and pairwise momentum balance of the two scatterings in DP events. A set of six variables with distinguishing power was identified. The first three are the ϕ angles between the photon and the three jets. The fourth, $E_T(1)/E_T(\gamma)$, the ratio of lead jet and photon E_T 's, is sensitive to the level of momentum balance between the two highest E_T objects. The fifth and sixth variables, S and ΔS , were used in the previous CDF analysis [5]. S represents the significance of pairwise momentum imbalance. It

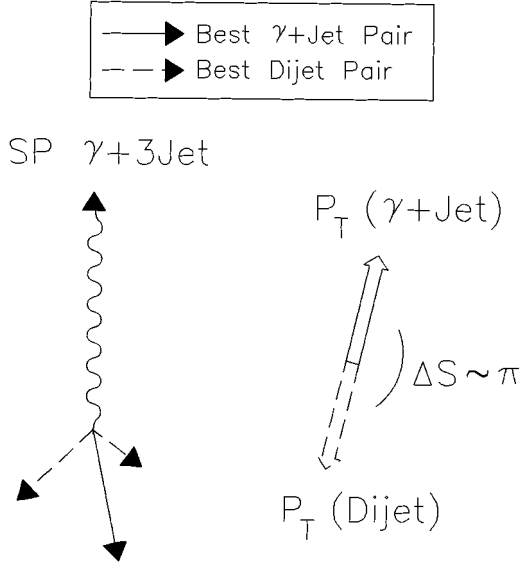


FIG. 5. Illustration of the definition of the ΔS variable, applied to a SP photon + 3 jet event. ΔS is the azimuthal angle between the p_T vectors of the two best-balancing pairs constructed from the photon + 3 jet system.

is also used to dissociate the $\gamma/\pi^0 + 3$ jet event into a $\gamma/\pi^0 + 1$ jet system and a dijet, based on the best achieved pairwise balance. The γ/π^0 and 3 jets are grouped into two pairs, $\gamma/\pi^0 + \text{jet } i$ and $\text{jet } j + \text{jet } k$, and the following quantity is formed:

$$S = \frac{1}{\sqrt{2}} \sqrt{\left(\frac{|\vec{p}_T(\gamma, i)|}{\delta p_T(\gamma, i)}\right)^2 + \left(\frac{|\vec{p}_T(j, k)|}{\delta p_T(j, k)}\right)^2}, \quad (7)$$

where $\vec{p}_T(\gamma, i)$ and $\vec{p}_T(j, k)$ are the transverse momenta of the two two-body systems and $\delta p_T(\gamma, i)$ and $\delta p_T(j, k)$ the corresponding uncertainties. Three pairings are possible, and the minimum S is selected. Most often in the data (87% of the time) S is minimized by pairing the photon with the highest E_T jet.

The last variable, ΔS , is the azimuthal angle between the p_T vectors of the minimum- S pairs. This is illustrated in Fig. 5. In SP events, momentum conservation biases ΔS towards 180° , while in DP events the ΔS distribution is flatter.

These six variables are kinematically correlated to one another to varying degrees. Correlations were tested using the PYTHIA and MIXDP models. For each model, events were weighted so as to produce significant changes in one of the distinguishing distributions. Changes in the remaining five distributions were then noted, and were found to be small on the scale of the differences in the distributions for the two models (Sec. VI).

VI. MEASUREMENT OF THE NUMBER OF DOUBLE PARTON EVENTS

Distributions of the six distinguishing variables for 1VTX data are shown in Fig. 6. Also shown for comparison are distributions from MIXDP (DP model) and PYTHIA (SP model). It is clear, most notably from the two variables with greatest sensitivity to DP, ΔS and $\delta\phi(\gamma, \text{jet } 1)$, that neither

model alone describes the data [21]. From a visual inspection of the six distributions, an admixture of approximately 50% DP + 50% PYTHIA (we write this as $f_{\text{DP}} = 50\%$) would best match the data in every case.

In previous analyses, DP was identified by an actual fit of kinematic distributions to admixtures of DP and SP Monte Carlo models. This approach introduces model dependence, specifically (applied to this analysis) on the PYTHIA prediction for SP, which is derived from theoretical calculations and phenomenological models which are uncertain. To avoid such model dependence, the number of DP events in the 1VTX data was determined using a background subtraction technique developed for this analysis. This technique statistically subtracts SP background from the 1VTX data through the use of a second CDF photon + 3 jet dataset, chosen to be somewhat poorer in DP. This “two-data-set” method does not invoke any prediction or model for the SP component of the data, but relies only on a comparison of the distributions of distinguishing variables for the two data samples and MIXDP.

We give here a brief outline of the two-data-set method, and provide a full description in Sec. VI A. Two $\gamma/\pi^0 + 3$ jet selection criteria are applied to data, such that the resulting data sets, A and B , differ in their signal fractions, i.e., in the ratio of the number of DP events to total events ($f_{\text{DP}}^A \neq f_{\text{DP}}^B$). Distributions of a distinguishing variable, for example ΔS , are plotted for both samples. The B plot is then scaled by a parameter k and subtracted from the A plot, with k varied until the “ $A - kB$ ” plot has the shape of the MIXDP prediction for this variable. With this value of k , the subtraction has cancelled the SP component of the A plot, leaving only the DP distribution. The values of f_{DP}^A and f_{DP}^B are then extracted from k . This method is illustrated in Fig. 7.

The DP-rich and DP-poor photon + 3 jet data sets were selected as follows. The A sample is the standard 1VTX dataset. The B sample is the same as A with a single change: we require $7 < [E_T(2), E_T(3)] < 9$ GeV instead of $5 < [E_T(2), E_T(3)] < 7$ GeV (Table I). Requiring higher jet energies reduces the DP to SP ratio. This is seen in Fig. 8(a), which compares $E_T(2)$ spectra for MIXDP and data events passing the 1VTX selection criteria, apart from the upper limit on $E_T(2)$ and $E_T(3)$. The ratio of spectra is plotted in Fig. 8(b). The second jet in MIXDP events is seen to have a softer spectrum than the data. Since the data are believed to be an admixture of DP and SP processes, we conclude that the E_T spectrum for DP jets is softer than the spectrum of the radiated jets in SP events [22]. This difference in spectra is the justification for the $E_T(2), E_T(3) < 7$ GeV selection requirement applied to the 1VTX and 2VTX event samples. Selecting elsewhere on this spectrum creates a dataset with a different signal fraction.

A. Description of the “two-data-set” method

The two-data-set technique is a general approach to the problem of identifying a signal with known properties amidst an unknown background. It operates by comparing distributions of distinguishing variables for two data sets, designed so that one data set is richer in signal than the other. The method is strictly valid only if the shapes of the background distributions in the two data sets are the same.

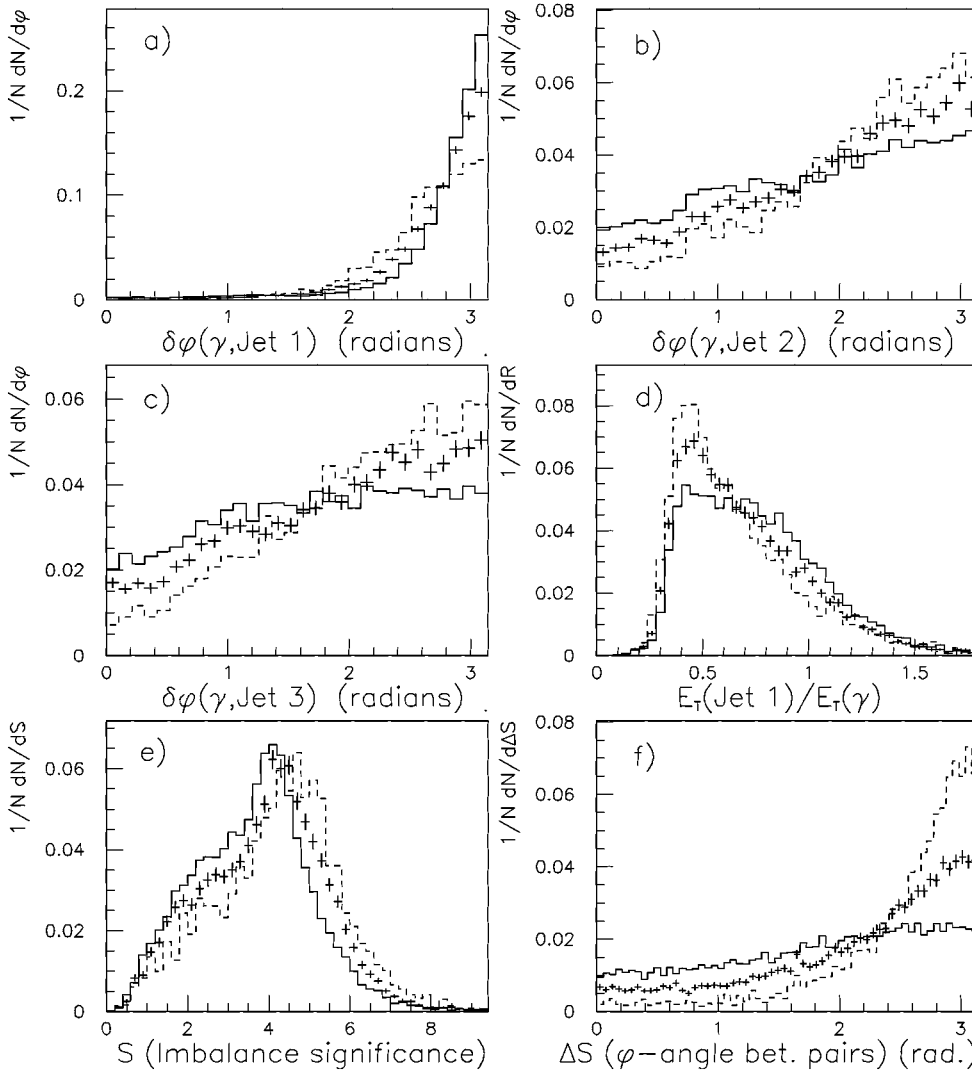


FIG. 6. The six sensitive kinematic variables plotted for 1VTX data (points), the MIXDP prediction for DP (solid), and the PYTHIA prediction for SP events (dashed).

For this analysis the two-data-set method operates on distributions for the A and B photon + 3 jet data sets. We assume that each distribution can be expressed as a sum of DP and SP distributions. In the DP-rich A data set, the distribution for any one of the variables, \mathcal{A} , is written $\mathcal{A}_i = (1 - f_{\text{DP}}^A) \mathcal{Q}_i + f_{\text{DP}}^A \mathcal{M}_i^A$ for each bin i , where \mathcal{Q} is the QCD SP background distribution (unknown), and \mathcal{M}^A is the distribution for MIXDP events passing the A selection. Similarly for the DP-poor B data set, $\mathcal{B}_i = (1 - f_{\text{DP}}^B) \mathcal{Q}_i + f_{\text{DP}}^B \mathcal{M}_i^B$. All distributions are normalized to unit area. We have assumed a common SP background distribution, \mathcal{Q} . To minimize the impact of this assumption, the two selection criteria were chosen to be similar, so as to maintain similar kinematic constraints in the two data sets. The assumption will also be tested directly (Sec. VI C).

Proceeding with the derivation of the method, we eliminate \mathcal{Q}_i from the equations for \mathcal{A}_i and \mathcal{B}_i and obtain

$$\mathcal{A}_i - \left(\frac{1 - f_{\text{DP}}^A}{1 - C f_{\text{DP}}^A} \right) \mathcal{B}_i = f_{\text{DP}}^A \mathcal{M}_i^A - \left(\frac{C f_{\text{DP}}^A (1 - f_{\text{DP}}^A)}{1 - C f_{\text{DP}}^A} \right) \mathcal{M}_i^B, \quad (8)$$

where $C \equiv f_{\text{DP}}^B / f_{\text{DP}}^A$. Remarkably, this ratio of signal fractions, C , is a known parameter (see below). Thus Eq. (8) can

be implemented as a χ^2 test over all bins of the four known plots, \mathcal{A} , \mathcal{B} , \mathcal{M}^A , and \mathcal{M}^B , with a single free parameter f_{DP}^A .

We now demonstrate how the C parameter is obtained. The two selection criteria, A and B , are applied to data and MIXDP. A total of N_A^{DATA} and N_A^{MIX} events survive the A selection, and N_B^{DATA} and N_B^{MIX} survive the B selection. One can formally write $N_A^{\text{MIX}} = \lambda N_A^{\text{DP}}$, with N_A^{DP} the unknown number of actual DP events in sample A , and λ an unknown parameter. If MIXDP models the properties of DP events, then for the B selection one can write $N_B^{\text{MIX}} = \lambda N_B^{\text{DP}}$, with the same value of λ . In other words, if MIXDP models DP accurately, then it models the relative efficiency for DP events to pass two selection criteria. Therefore,

$$C \equiv \frac{f_{\text{DP}}^B}{f_{\text{DP}}^A} \equiv \left(\frac{N_B^{\text{DP}}}{N_B^{\text{DATA}}} \right) \left(\frac{N_A^{\text{DATA}}}{N_A^{\text{DP}}} \right) = \left(\frac{\lambda N_B^{\text{DP}}}{N_B^{\text{DATA}}} \right) \left(\frac{N_A^{\text{DATA}}}{\lambda N_A^{\text{DP}}} \right) = \left(\frac{N_B^{\text{MIX}}}{N_B^{\text{DATA}}} \right) \left(\frac{N_A^{\text{DATA}}}{N_A^{\text{MIX}}} \right). \quad (9)$$

The C parameter is thus determined without knowledge of the actual amount of DP in data. Given the two selection criteria, we find $N_A^{\text{DATA}} = 16\,853$, $N_B^{\text{DATA}} = 3727$, N_A^{MIX}

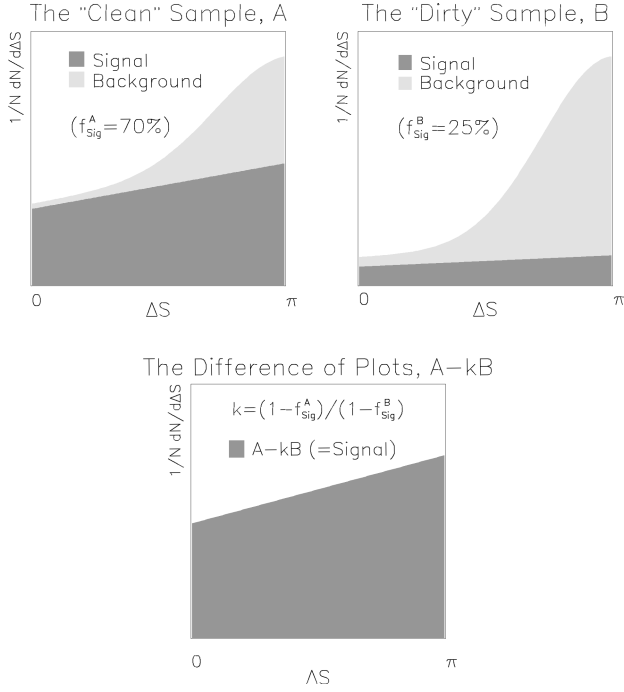


FIG. 7. The “two-data-set” method for extracting f_{DP} , illustrated for two hypothetical data samples A and B . ΔS distributions for the two data sets, normalized to unit area, are shown. In the A sample, DP (“signal”) constitutes 70% of the sample, while in the B sample DP is 25%. The DP component of each plot is shown in heavy shading, the SP background (“background”) in light shading. The scaled difference of the two distributions, $A - kB$, is also shown, with k such that the SP component of the A distribution has been subtracted off. The $A - kB$ distribution is then equal to the DP distribution alone.

$= 21\,240$, and $N_B^{\text{MIX}} = 3105$. Thus $C = 0.660 \pm 0.002$. In other words, the B data set has a signal fraction 66.0% the size of the signal fraction in the A set.

B. Results of the “two-data-set” method

The two-data-set technique was applied to the distributions of the four angle-based distinguishing variables. The E_T ratio and S variables were not suitable for this method, since their distributions depend on the lower limit on $E_T(2)$, which is different for the A and B samples. Results are given in Table II. The simultaneous fit to all four variables has a reasonable χ^2 (167.6/149 DF) and yields $f_{\text{DP}}^A \equiv f_{\text{DP}} = (52.6 \pm 2.5)\%$. Fits to the individual distributions are also listed [23].

Results of this simultaneous fit are shown graphically in Figs. 9–12 for the four variables. Figures 9(a)–12(a) show distributions for the A selection for both data and MIXDP,

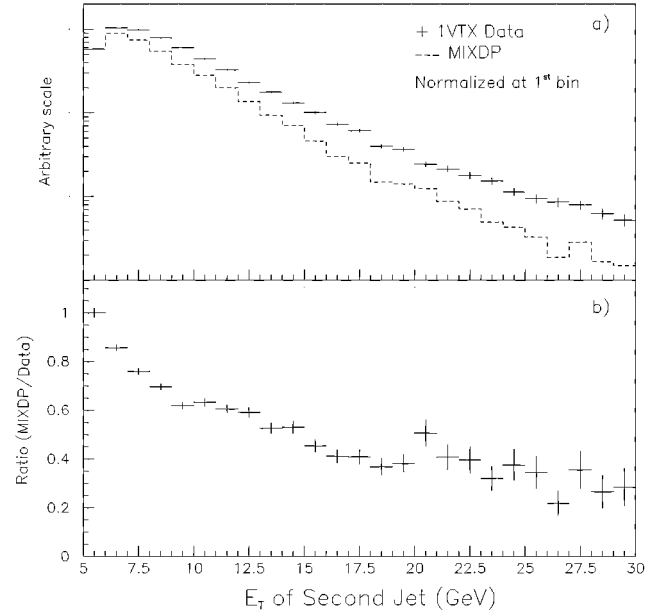


FIG. 8. (a) The $E_T(2)$ distributions for data passing the 1VTX selection criteria apart from the upper limit on $E_T(2), E_T(3)$ (points), and for events from the MIXDP model (dashed histogram). The two spectra have been normalized at the first bin. (b) Ratio of the two spectra, MIXDP/data.

with MIXDP normalized to $f_{\text{DP}} = 52.6\%$ of the area. Figures 9(b)–12(b) show the same for the B selection, with MIXDP normalized to $f_{\text{DP}}^B = 0.660 \times 52.6\% = 34.7\%$ of the area. The next two sets of plots are consistency checks of the two-data-set method. Figures 9(c)–12(c) show the “ $A - kB$ ” distributions [the LHS of Eq. (8)] which should match the MIXDP predictions [the RHS of Eq. (8)]. The agreement is generally good, as reflected by the fit χ^2 values. Figures 9(d)–12(d) show the “extracted SP” shapes for A and B , obtained by subtracting the MIXDP distribution from the data distribution, for both data sets. This is a check of the assumption that the two SP distributions have the same shape. Only minor evolution in the extracted SP shapes is seen.

C. Checks of the two-data-set method

In a more quantitative test of whether the assumption of a common SP background shape is valid, as well as to check the overall robustness of the method, the two-data-set technique was applied to mock data constructed from MIXDP and PYTHIA events. Note that the PYTHIA model provides a prediction for possible differences in the SP distributions for the A and B selections. Input MIXDP fractions ranged from 35%

TABLE II. Results for the fraction of double parton events (%) in the 1VTX data, obtained from the two-dataset method. The associated χ^2 's and numbers of degrees of freedom are also shown.

	Distinguishing variable tested:				
	$\delta\phi(\gamma_{\text{jet } 1})$	$\delta\phi(\gamma_{\text{jet } 2})$	$\delta\phi(\gamma_{\text{jet } 3})$	ΔS	All
$f_{\text{DP}} (\%)$	61.5 ± 4.0	20.2 ± 15.3	53.9 ± 6.3	51.1 ± 3.6	52.6 ± 2.5
$\chi^2/(\text{No. DF})$	41.5/29	27.4/29	18.0/29	69.2/59	167.6/149

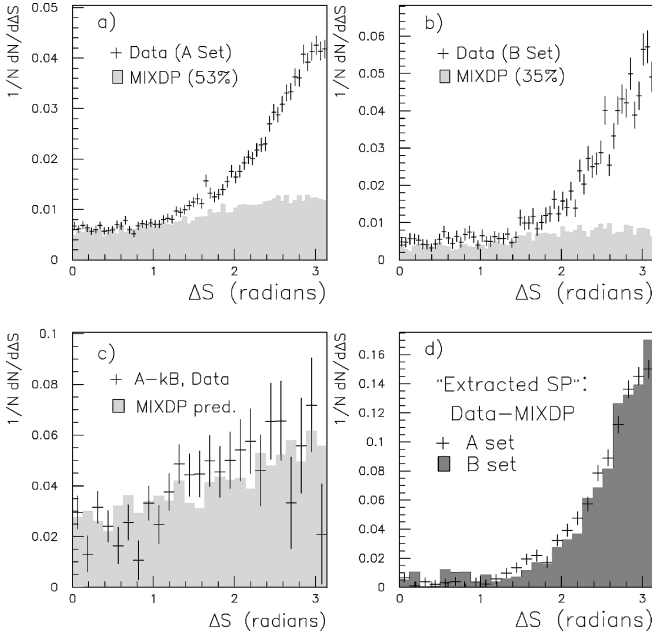


FIG. 9. Results for the two-data-set fit to the ΔS distribution. The simultaneous fit value, $f_{DP} = 52.6\%$, has been used. (a) Distributions for the A selection, data (points) and MIXDP (shaded), with MIXDP normalized using f_{DP} . (b) Same, for the B selection; MIXDP is normalized using $0.66 \times f_{DP}$. (c) “A-kB,” the difference of the data distributions in (a) and (b), scaled so as to best eliminate the SP contribution to A. This is compared to the pure MIXDP prediction (shaded). (d) The SP distributions in the A and B sets, obtained by subtracting MIXDP (normalized by f_{DP} and $0.66 \times f_{DP}$, respectively) from the data.

to 65%. The resulting measured fractions tracked the input fractions well. For example, the data set with input fraction 50.6% was found as having $(51.3 \pm 2.0)\%$ DP. Results are shown graphically in Fig. 13. No systematic bias to the extracted fractions was observed within the statistics of the

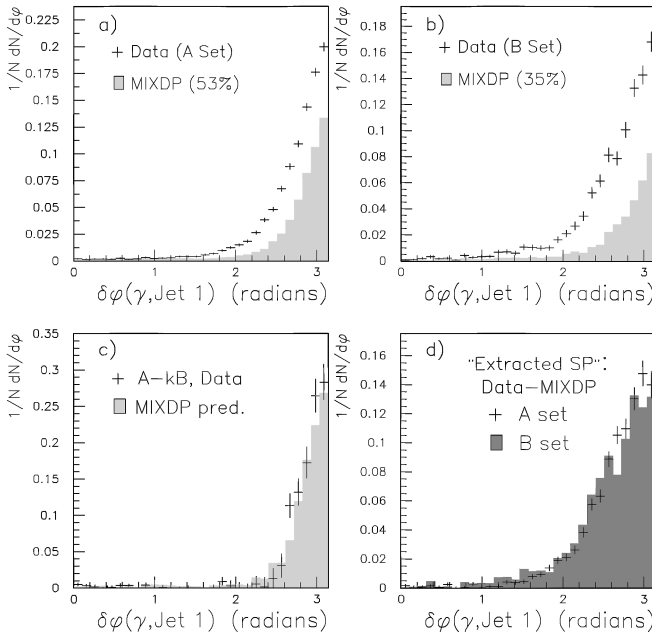


FIG. 10. Results for the two-data-set fit to the $\delta\phi(\gamma, \text{jet 1})$ distribution. See Fig. 9 for description.

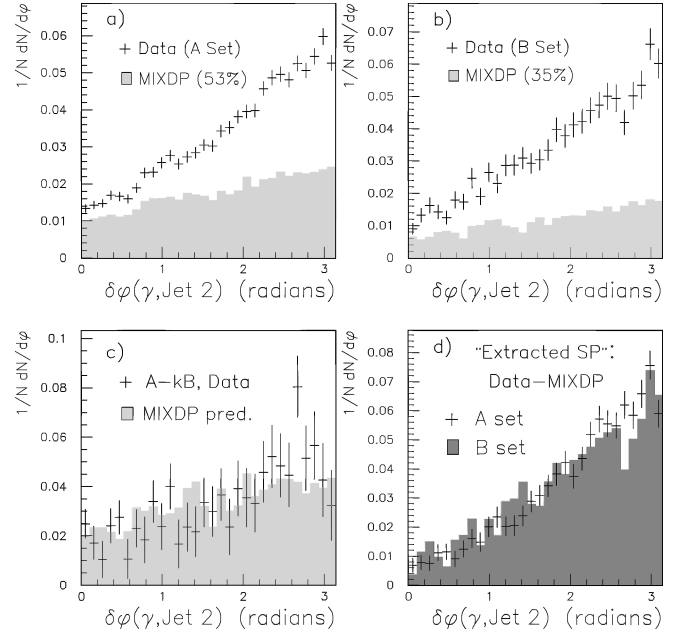


FIG. 11. Results for the two-data-set fit to the $\delta\phi(\gamma, \text{jet 2})$ distribution. See Fig. 9 for description.

mock samples. A linear fit to the found vs true DP fractions and its statistical uncertainties was performed. Based on this fit, systematic uncertainty is assigned to the f_{DP} value obtained for the 1VTX data. We find $f_{DP} = [52.6 \pm 2.5(\text{stat.}) \pm 0.9(\text{syst.})]\%$.

As a check of this large DP fraction, the admixture 52.6% MIXDP+47.4% PYTHIA is compared to 1VTX data in Fig. 14. All six distinguishing variables are shown. In each case, the data are well described by this admixture. Figure 15 shows the comparison for the ΔS variable alone, which has the greatest sensitivity to DP. We note that a simultaneous PYTHIA+MIXDP fit to the six distributions yields f_{DP}

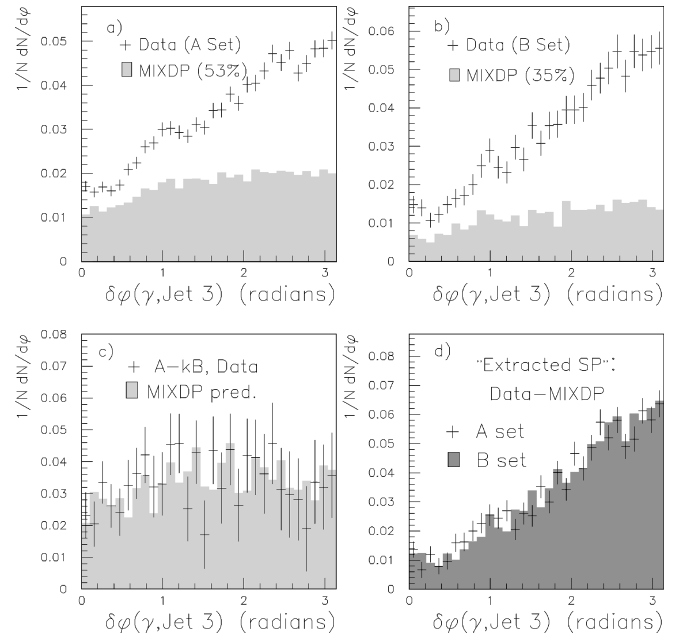


FIG. 12. Results for the two-data-set fit to the $\delta\phi(\gamma, \text{jet 3})$ distribution. See Fig. 9 for description.

$= (51.8 \pm 1.0)\%$ (statistical uncertainty), a result that is indistinguishable from the two-data-set result, since the fit χ^2 is the same as for a constrained fit to $f_{\text{DP}} = 52.6\%$ ($273.0/244 N_{\text{DF}}$).

D. The number of DP events

Before calculating N_{DP} , the number of DP events, a correction must be applied for the possible presence of triple parton scattering events, which because of similar kinematics would appear as part of the observed double parton signal. This correction is necessary because the σ_{eff} extraction technique (Sec. II) relies explicitly on Eq. (1), which we take to be the cross section for two and only two pairs of parton scatterings. MIXDP events were used to determine the correction, based on the possible presence of double parton scattering in the two ingredient event samples. This is described in Appendix B. We estimate that $17^{+4}_{-8}\%$ of the observed DP signal is triple parton scattering, necessitating that the signal be reduced by a factor of $0.83^{+0.08}_{-0.04}$.

It must also be noted that DI is potentially a second source of background to DP, since not all NSD $\bar{p}p$ collisions are found by the VTX. Based on the analysis of the DI component to the 2VTX data, described in the following section, we find that the contamination of DI events into the 1VTX DP signal is negligible [24], and make no correction. Taking together the number of 1VTX events, f_{DP} , and the correction for triple parton scattering, we obtain $N_{\text{DP}} = 7360 \pm 360^{+720}_{-380}$.

VII. MEASUREMENT OF THE NUMBER OF DOUBLE INTERACTION EVENTS

The number of DI events in the 2VTX sample must be determined in order to extract the σ_{eff} parameter [Eq. (6)]. To obtain N_{DI} , we exploit the fact that the jets in photon + 3 jet DI events originate from separate $\bar{p}p$ collisions [Figs. 3(b) and 3(c)]. The origins of jets along the beam line were determined using charged particle information from the CTC. The algorithm for finding jet origins operated as follows. (1) Jets were required to have $|\eta| < 1.3$ in order for associated charged particles to be within the volume of the CTC. (2) All CTC tracks whose (η, ϕ) lay within a cone $\Delta R < 0.7$ around the jet direction were considered as candidates for belonging to that jet. (3) The average z of these tracks was calculated. (4) The track with the largest deviation from the mean was removed and a new mean calculated; the process was repeated until no track had a maximum deviation exceeding 3.0 cm. (5) The jet origin in z was defined as the average z of the remaining tracks. For jets with $|\eta| < 1.1$, at least one track surviving the algorithm was required; if $1.1 < |\eta| < 1.3$, 2 such tracks were required.

As a test, the algorithm was applied to the 1VTX data sample. The difference between the z origin of the jets and the VTX vertex is shown in Fig. 16(a). Nearly all jet origins are found to be within 3 cm of the event vertex. This is not an artifact of the 3 cm “outlier” cut. Distributions of the number of accepted tracks per jet are shown in Figs. 16(b)–16(d) for the three jets. Even for the lowest E_T jet, at least one track is found roughly 90% of the time.

The algorithm was next applied to a sample of two vertex

events. The event sample for the jet origin analysis differed from the standard 2VTX sample in the following ways. A requirement of $|\eta| < 1.3$ was made for all three jets, and the two VTX vertices were required to be separated by at least 10 cm. The latter cut reduces confusion in the CTC track finding algorithm. In addition, to increase the size of the sample, the upper bound on the E_T of the two least energetic jets was removed. The total number of events passing these requirements and the jet tracking algorithm is 1333. The impact of these differences in selection criteria is discussed below.

In Fig. 17 we plot the difference in z origins for jets 1 and 3 (Δz_{13}) vs jets 1 and 2 (Δz_{12}). The data clearly divide into four classes: (1) Δz_{12} and $\Delta z_{13} < 5$ cm; (2) $\Delta z_{12} < 5$ cm and $\Delta z_{13} > 5$ cm; (3) $\Delta z_{13} < 5$ cm and $\Delta z_{12} > 5$ cm; (4) $|\Delta z_{12} - \Delta z_{13}| < 5$ cm. There are virtually no other events in the sample. In the absence of algorithmic failures or confusion, these classes would correspond to the following processes: (1) photon + 3 jets (SP or DP) from one collision; (2) DI, with jets 1,2 from one collision and jet 3 from the other; (3) DI, with jets 1,3 from one collision and jet 2 from the other; (4) DI, with jets 2,3 from one collision and jet 1 from the other. Experimentally, however, the classes and processes mix. Errors in jet origin determination occur when jets actually have few or no observable tracks, but are assigned an origin based on tracks from the second collision. We account for this effect by running the algorithm on events from the DI (MIXDI) and background (MIX2V) models that pass the selection criteria of the jet origin analysis. The algorithm performance on data and models, specifically the breakdown of events into their class assignments, is shown in Table III. If the algorithm were perfect, then all MIXDI events would be assigned to classes 2,3,4 (DI signal) and all MIX2V events would be assigned to class 1 (multiple collision background). In practice, the performance on the models indicates that the misidentification of the DI process as a multiple collision background, and *vice versa*, occurs at the level of 20%.

The numbers of data events found in the four classes were simultaneously fit to an admixture of MIXDI and MIX2V. The data are best described with a $(16.8 \pm 1.9)\%$ DI component, meaning that jets originate at separate $\bar{p}p$ collisions in this fraction of the two vertex event sample. The uncertainty is statistical. This result for the DI component is verified in Fig. 18, which compares ΔS distributions for events where all jets have a common origin (class 1) and for events with jets at separated origins (classes 2, 3, 4). A clear difference between the two classes is seen. The strong peaking near π seen in class 1 is typical for SP, whereas the flatter shape seen in the class 2, 3, and 4 category is indicative of the DI process. The shaded histograms are predictions, obtained by combining results from MIXDI and MIX2V in the ratio $f_{\text{DI}} = 0.168$. Good agreement is observed. ΔS distributions for the four classes are shown individually in Fig. 19, and agreement with the predictions is again good.

The number for the DI fraction obtained above pertains to an event sample that differs from the standard 2VTX dataset. We described in Sec. VI A a general technique for calculating the ratio of signal fractions in two data sets with different selection criteria [Eq. (9)]. Applying this, we find that the 16.8% DI fraction found in this study implies $f_{\text{DI}} = 17.7\%$

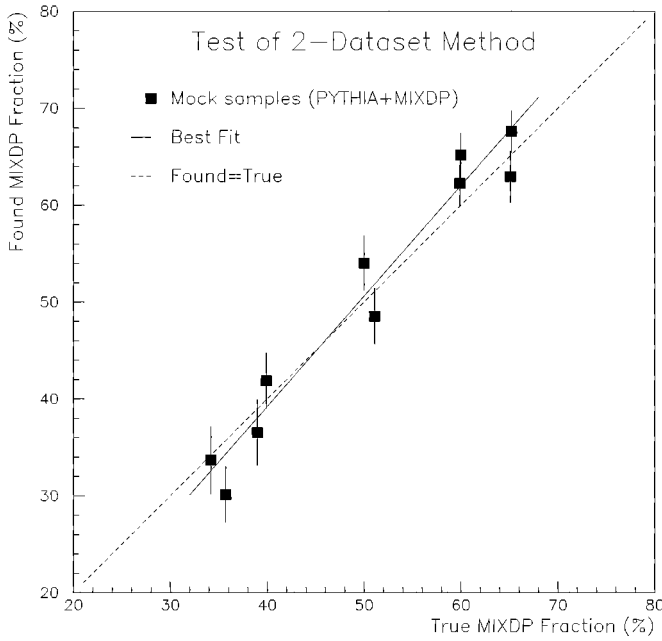


FIG. 13. Results for the test of the two-data-set method on mock data constructed from MIXDP and PYTHIA events. The MIXDP fraction was varied from 35% to 65%.

for the standard 2VTX sample. This translation has negligible uncertainty.

To test the robustness of this value for f_{DI} , the selection criteria for the jet-tracking sample were varied. The requirements on jet η and the number of associated tracks were relaxed and tightened on both data and the mixed models. The extracted values of f_{DI} agreed to 10%, fractionally, and no trend was observed within statistics. We therefore take $f_{\text{DI}} = (17.7 \pm 1.9 \pm 1.8)\%$. Other possible sources of uncertainty, such as misassignment of vertices for the calculation of jet η , and tracking confusion in events with close vertices, have been investigated and are small. Taken together with the number of 2VTX events, we obtain $N_{\text{DI}} = (1060 \pm 110 \pm 110)$.

VIII. EXTRACTING THE σ_{eff} PARAMETER

The first-order expression for extracting σ_{eff} from the comparison of the number of DP and DI events was given in Eq. (6). To obtain a more realistic expression we include (1) kinematic acceptance for DP and DI events to enter our event samples, and (2) efficiencies for a beam crossing with n collisions to be observed as having 1 VTX vertex (DP candidates) or 2 VTX vertices (DI candidates). The vertex efficiency correction accounts for single (double) collision

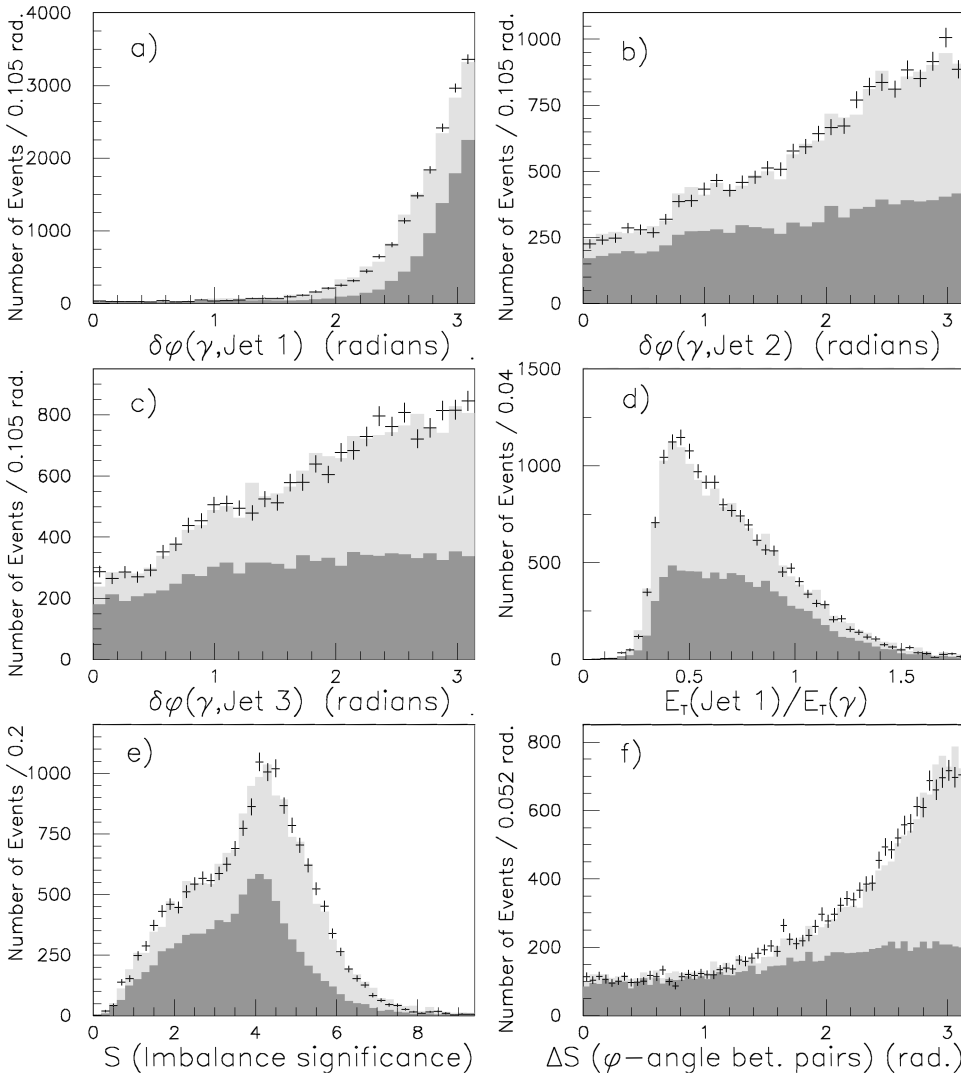


FIG. 14. Comparison of the six distinguishing kinematic variables for 1VTX data (points) and a 52.6%/47.4% admixture of DP (MIXDP) and SP (PYTHIA) models. The MIXDP component is shown in heavy shading, the PYTHIA component in light shading. The level of the DP component was determined by the PYTHIA-independent two-data-set method.

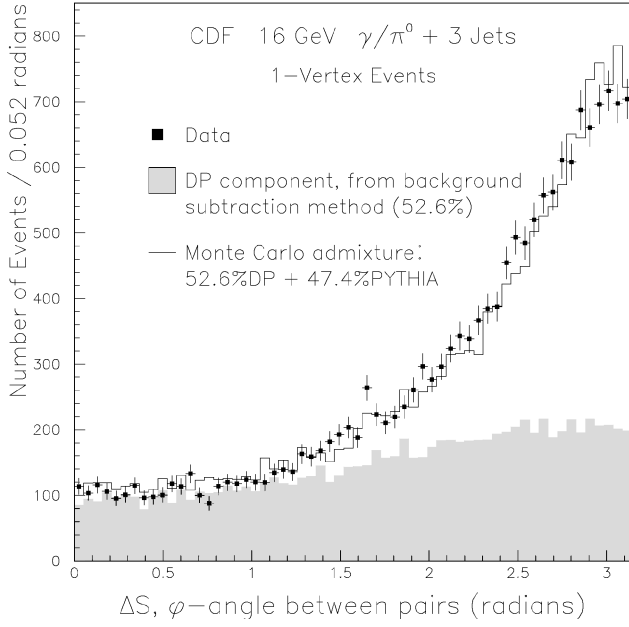


FIG. 15. ΔS distribution for 1VTX data (points). The DP component to the data, determined by the two-data-set background subtraction method to be 52.6% of the sample, is shown as the shaded region (the shape is taken from MIXDP). Also shown is the admixture 52.6% MIXDP+47.4% PYTHIA, normalized to the data (line).

events lost from the DP (DI) candidate sample, and for events with more than one (two) collision(s) which contribute to the DP (DI) sample. These modifications are described in Appendix C. The updated expression for σ_{eff} is

$$\sigma_{\text{eff}} = \left(\frac{N_{\text{DI}}}{N_{\text{DP}}} \right) \left(\frac{A_{\text{DP}}}{A_{\text{DI}}} \right) (R_c) (\sigma_{\text{NSD}}). \quad (10)$$

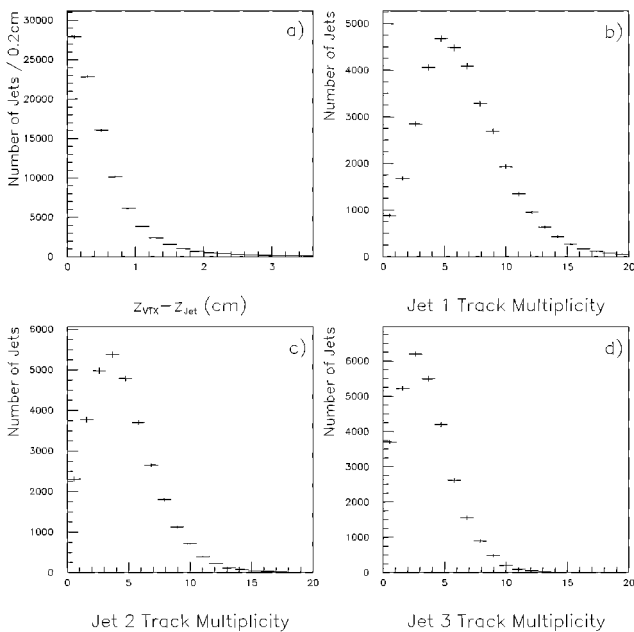


FIG. 16. Results of the jet tracking study on single vertex $\gamma/\pi^0 + 3$ jet events. (a) Separation between the VTX vertex and the jet origins in z . (b)–(d) Charged track multiplicity for the jets.

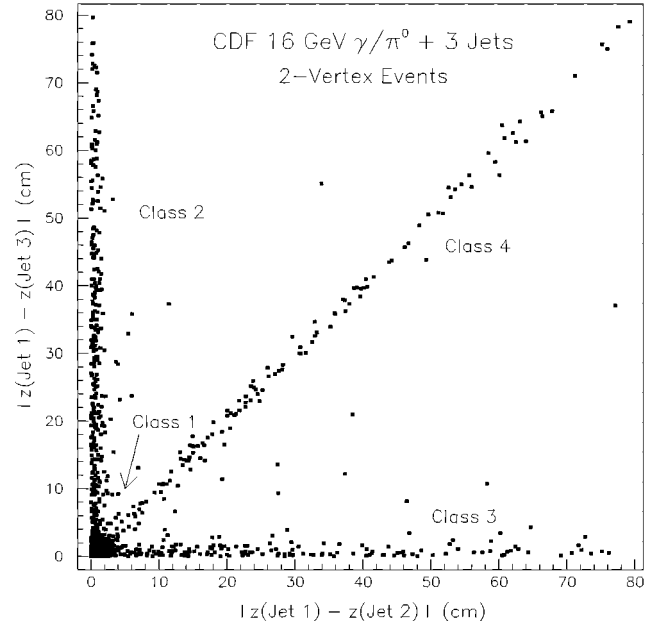


FIG. 17. Scatterplot of the difference in z origin for jets 1 and 3 (Δz_{13}) vs jets 1 and 2 (Δz_{12}), in $\gamma/\pi^0 + 3$ jet events with two vertices. The data are subdivided into four classes. Double interaction events, in which jets are produced at separate $\bar{p}p$ collisions, should appear in classes 2, 3, and 4.

The acceptances for DP and DI events to pass kinematic selection requirements, apart from the vertex selection, are denoted by A_{DP} and A_{DI} . The factor R_c replaces the ratio $N_c(1)/[2N_c(2)]$ found in Eq. (6), and is a function of the number of beam crossings with n collisions, $N_c(n)$, and VTX vertex identification efficiencies; see Appendix C.

The ratio of kinematic acceptances in Eq. (10) was obtained by taking the ratio of accepted events from MIXDP and MIXDI event mixing, operating on the same samples of ingredient events. The different levels of underlying event in single and double $\bar{p}p$ collision events result in different jet-finding efficiencies and jet multiplicities, and thus different acceptances. For example, the higher level of this energy in DI events (1) reduces the efficiency for passing the photon trigger isolation cut, (2) makes it easier to find three jets above 5 GeV and thus accept the event, and (3) makes it

TABLE III. Performance of the jet origin algorithm operating on two-vertex $\gamma/\pi^0 + 3$ jet data and on models for DI (MIXDI) and multiple collision background (MIX2V). The breakdown of the number of events into the four origin classes (Sec. VII) is shown for each of the three samples tested. Based on the numbers in the MIXDI and MIX2V columns, the jet origin algorithm misidentification rate (DI found as multiple collision background, and *vice versa*) is approximately 20%.

Event class	# Data events per class	Frac. of samples assigned to each class		
		Data	MIXDI	MIX2V
1	946	0.710	0.224	0.813
2	185	0.138	0.353	0.090
3	105	0.079	0.190	0.064
4	97	0.073	0.233	0.033

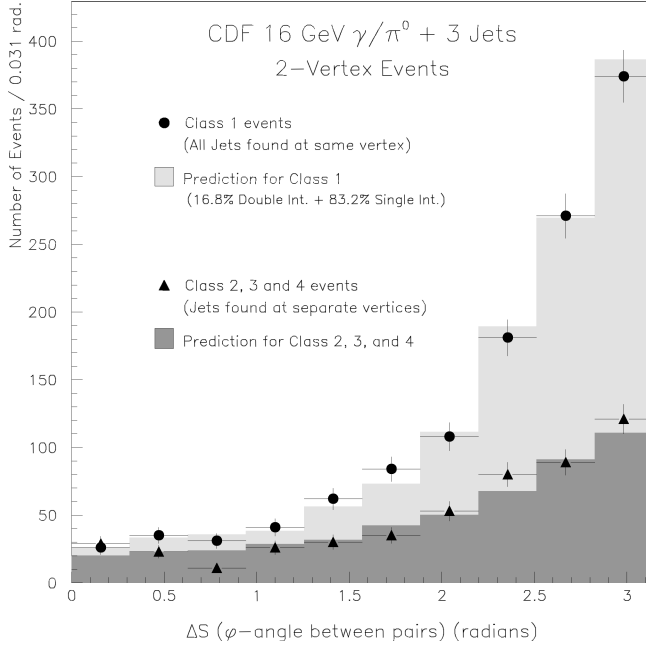


FIG. 18. ΔS distributions for class 1 and class 2+3+4 jet origin categories, in 2 vertex $\gamma/\pi^0 + 3$ jet events. The shaded plots are predictions based on MIXDI and MIX2V events, using $f_{\text{DI}} = 0.168$.

easier to find more than three jets above 5 GeV and thus reject the event. We find $A_{\text{DP}}/A_{\text{DI}} = 0.958$ with negligible statistical uncertainty. Apart from the fact that MIXDP explicitly models uncorrelated DP scattering, systematic uncertainty on the mixing models and the acceptance ratio is small.

The number of beam crossings with n collisions, $N_c(n)$, is needed for the evaluation of the R_c term in Eq. (10). It was obtained from σ_{NSD} and the instantaneous luminosities

($\mathcal{L}_{\text{inst}}$) for the 1992–3 Tevatron Run. For a given $\mathcal{L}_{\text{inst}}$ the number of NSD collisions per crossing is a Poisson distribution with mean $\langle n \rangle = (\mathcal{L}_{\text{inst}}/f_0)(\sigma_{\text{NSD}})$, with f_0 the frequency of beam crossings at the Tevatron. $N_c(n)$ was evaluated as a sum of Poisson distributions with different means, based on the $\mathcal{L}_{\text{inst}}$ distribution. The first several terms of $N_c(n)$, expressed as fractions of the total number of crossings, are $N_c(1) = 27.2\%$, $N_c(2) = 7.25\%$, $N_c(3) = 1.55\%$. This means, for example, that 27.2% of the beam crossings in the 1992–3 CDF data are predicted to have one and only one NSD $\bar{p}p$ collision.

The first-order expression for the R_c term, as it appears in Eq. (6), is $N_c(1)/[2N_c(2)]$. Given the above, it has the value 1.87. Using the full expression for R_c in terms of $N_c(n)$ and VTX efficiencies, as it appears in Appendix C, we find $R_c = 2.06 \pm 0.02^{+0.01}_{-0.13}$. The second uncertainty is systematic, and is also derived in Appendix C.

The final parameter in Eq. (10) is the NSD cross section. This was derived from the CDF measurements of Ref. [9] by subtracting the single-diffractive cross section (9.46 ± 0.44 mb) from the inelastic cross section (60.33 ± 1.40 mb). We obtain $\sigma_{\text{NSD}} = (50.9 \pm 1.5)$ mb.

Inserting these values into Eq. (10), our measurement of the process-independent parameter of double parton scattering is $\sigma_{\text{eff}} = (14.5 \pm 1.7^{+1.7}_{-2.3})$ mb.

IX. IMPLICATIONS OF THE σ_{eff} MEASUREMENT, AND KINEMATIC STUDIES

The σ_{eff} parameter of double parton scattering contains information on the spatial distribution of partons within the proton and on possible correlations between the partons. In the remainder of this paper we investigate these issues. In Sec. IX A the measured σ_{eff} is used to constrain various models of parton spatial density. In Sec. IX B we ask whether this density, and thus σ_{eff} , is dynamic. In Sec. IX C a search for kinematic correlations between the two scatterings in DP events is described.

A. Parton spatial density

In Sec. I we mentioned that a simple model of proton structure predicted a value of 11 mb for σ_{eff} . Our measured value of $(14.5 \pm 1.7^{+1.7}_{-2.3})$ mb is consistent with this expectation. We now describe this prediction, and investigate predictions from other models of proton structure.

A strictly classical approach for calculating σ_{eff} given a spatial distribution of partons was taken from Ref. [25]. Given a density, the overlap integral of the product of the proton and antiproton parton spatial densities was evaluated, for a $\bar{p}p$ collision with impact parameter Δ . This quantity, $D(\Delta)$, is taken to be proportional to the “parton-parton luminosity” for single hard scatterings in collisions with this impact parameter. Individual hard scattering cross sections are thus proportional to $D(\Delta)$, while the cross section for two parton-parton hard scatterings is proportional to its square. In light of Eq. (1), the expression for σ_{eff} is

$$\sigma_{\text{eff}} = \frac{1}{2} \frac{\left[\int_0^\infty D(\Delta) 2\pi \Delta d\Delta \right]^2}{\int_0^\infty D(\Delta)^2 2\pi \Delta d\Delta}. \quad (11)$$

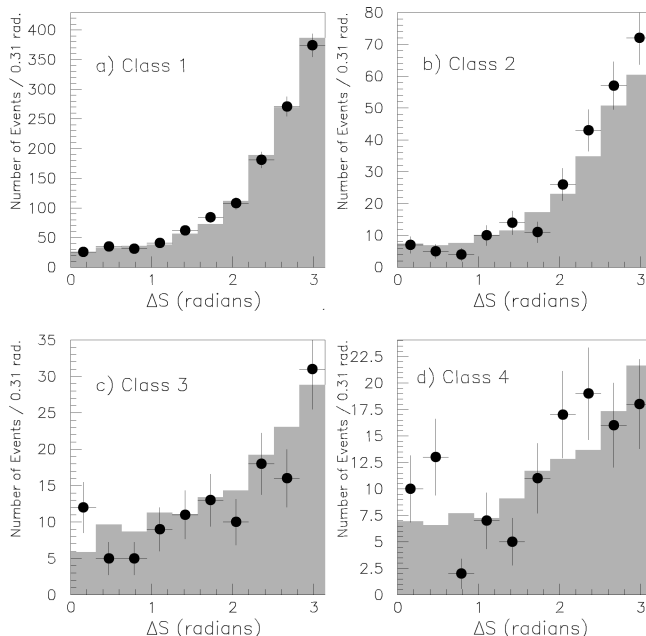


FIG. 19. ΔS distributions for the four jet origin classes, in two vertex $\gamma/\pi^0 + 3$ jet events. The shaded plots are predictions based on MIXDI and MIX2V events, using $f_{\text{DI}} = 0.168$.

TABLE IV. Results from the parton spatial density analysis. Predictions for rms radius and σ_{eff} are shown for several density models. Equating the σ_{eff} predictions to the measured value of σ_{eff} determines the distance scale parameters. Also, rms radii are derived from the distance scales. The cutoff parameter for each model, n , defines an effective radius for NSD collisions, and is obtained from the distance scale, the relation $\sigma_{\text{NSD}} \equiv \pi(2n \times \text{scale})^2$, and the CDF measurement of σ_{NSD} . The measured distance scales, rms radii, and cutoffs have $\pm 10\%$ uncertainty (statistical and systematic in quadrature).

Model for density	Form of density, dN/d^3r	Predictions		Measurements		
		rms r	σ_{eff}	Scale (fm)	rms r (fm)	n
Solid sphere	Constant, $r < r_p$	$\sqrt{3/5}r_p$	$4\pi r_p^2/4.6$	$r_p = 0.73$	0.56	0.87
Gaussian	$e^{-r^2/2\Sigma^2}$	$\sqrt{3}\Sigma$	$4\pi\Sigma^2$	$\Sigma = 0.34$	0.59	1.9
Exponential	$e^{-r/\lambda}$	$\sqrt{12}\lambda$	$35.5\lambda^2$	$\lambda = 0.20$	0.70	3.2
Fermi, $\lambda/r_0 = 0.2$	$(e^{(r-r_0)/\lambda} + 1)^{-1}$	$1.07r_0$	$4.6r_0^2$	$r_0 = 0.56$	0.60	1.1
Fermi, $\lambda/r_0 = 0.5$	“ ”	$2.01r_0$	$14.5r_0^2$	$r_0 = 0.32$	0.63	2.0
Fermi, $\lambda/r_0 = 0.8$	“ ”	$3.05r_0$	$32.8r_0^2$	$r_0 = 0.21$	0.64	3.0

The integrals are over all impact parameters, assuming azimuthal symmetry. The partonic cross sections for the two scatterings, such as $\hat{\sigma}_A$ and $\hat{\sigma}_B$ in Fig. 1, cancel in Eq. (11). The factor of 1/2 comes from the definition of σ_{eff} [Eq. (1)].

Equation (11) was evaluated for the simplest “solid sphere” model, which assumes spherical protons (radius r_p) with a uniform parton density. We find $\sigma_{\text{eff}} = 4\pi r_p^2/4.6$. Using the measured σ_{eff} we extract a proton radius of (0.73 ± 0.07) fm, where statistical and systematic uncertainties have been added in quadrature.

The solid sphere model for proton structure also has the unique feature that it predicts both σ_{eff} and σ_{NSD} . In this model the NSD cross section is equal to $\pi(2r_p)^2$, meaning that any scattering in which the spheres “touch” contributes to σ_{NSD} . Thus $\sigma_{\text{eff}} = \sigma_{\text{NSD}}/4.6$, and one can use the measured value for σ_{NSD} to obtain a numerical prediction for σ_{eff} . The value of 11 mb mentioned in Sec. I was obtained in this way. The factor of 4.6 is a purely geometric enhancement of the DP cross section: because single parton-parton scatterings occur with highest probability in small impact-parameter $\bar{p}p$ collisions, where the overlap of parton densities is largest, the probability for a second scattering given the first is enhanced.

Three other models for the parton density distribution—Gaussian, exponential, and Fermi—have also been tested. The Fermi model is analogous to the charge density distribution seen in heavy nuclei [26]. The predictions for σ_{eff} , obtained from Eq. (11), are functions of the distance-scale parameter for each model. In the same way that r_p was extracted from the solid sphere model, we use the measured σ_{eff} to determine the scale parameters. Results are summarized in Table IV.

These results can be compared to venerable measurements of proton size from ep elastic scattering. The relevant quantity determined in these experiments was the rms radius of the proton charge distribution, found to be (0.77 ± 0.10) fm in scatterings with momentum transfer Q^2 of order 0.1–0.5 GeV² [26]. To compare with this value, the distance-scale parameters obtained from the density models were converted to rms radii. The relationships between parameter and rms radius, and the resulting rms radii, are listed in Table IV. Despite the difference in Q^2 between the experiments, these rms radii are consistent with the ep scatter-

ing value. It is interesting that similar rms radii values are obtained from the different density models.

The Fermi, exponential, and Gaussian models do not predict σ_{NSD} , because they lack a natural cutoff of the density in radius. For these models we have taken an opposite approach, and have used the measured σ_{NSD} to specify the effective proton radius corresponding to NSD interactions. In particular, we express this “NSD radius” as a multiple of the distance-scale parameter of each distribution. For example, in the case of the exponential distribution of partons, where $dN \propto e^{-r/\lambda} d^3r$, we determine λ using σ_{eff} as before, then assume $\sigma_{\text{NSD}} \equiv \pi(2n\lambda)^2$ and solve for n . By this definition, $n\lambda$ is the effective proton radius for NSD collisions. These cutoff parameters are also given in Table IV.

B. Feynman x dependence and x correlations

The σ_{eff} value from the present analysis agrees well with the previous best measurement of $12.1^{+10.7}_{-5.4}$ mb. However, if σ_{eff} were a function of the kinematics of the scatterings involved, the two measurements would not be expected to coincide. For example, a dynamic parton spatial density, where the density depends on the Feynman x of the partons ($x \equiv p_{\text{parton}}/p_{\text{beam}}$), would generate an x -dependent σ_{eff} . As an illustration, consider a model in which higher x partons are concentrated in a “hot core” within the proton. At higher x the effective proton size, and thus σ_{eff} , would be smaller, resulting in a DP cross section enhanced for scatterings at high x relative to low x .

The possible Feynman x dependence of σ_{eff} was studied by searching for deviations from the MIXDP model, which by construction has the x dependence of the two scatterings only. It is worth noting that, although the analysis of Sec. VI indicates that DP events in data have several properties that are well described by MIXDP, this does not rule out an x -dependent σ_{eff} . The primary manifestation of such a dependence would be in the DP rate vs x , with possibly negligible effects on other kinematic properties of the photon + 3 jet system.

We begin by establishing an enriched sample of DP candidate events, consisting of 1VTX data that pass the cut $\Delta S < 1.2$ (2575 events). Based on the MIXDP+PYTHIA curve shown in Fig. 14(f), the data passing this cut should be 90% DP. Each event was subdivided as usual into the two best-

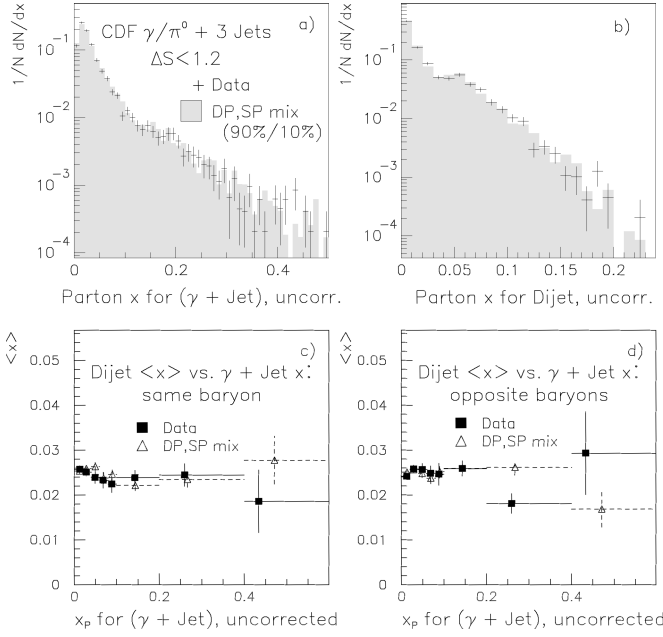


FIG. 20. Results of the Feynman x analysis. Distributions of (a) x for the γ +1 jet system ($x_{p,p}^{\gamma J} \equiv [p_T^{\gamma}/p_{\text{beam}}][e^{\pm}\eta_{\gamma} + e^{\pm}\eta_J]$), and (b) x for the dijet system ($x_{p,p}^{JJ} \equiv \{[E_T(i) + E_T(j)]/(2p_{\text{beam}})\}[e^{\pm}\eta_i + e^{\pm}\eta_j]$, where i, j signify the two jets of the dijet). Two entries are made in each plot per event, one for each of the two partons contributing to the particular two-body system. The prediction, 90% MIXDP+10% PYTHIA, is shown as the shaded area. Events were required to have $\Delta S < 1.2$. A correlation study is also shown: average x for the dijet system plotted against x of the γ +1 jet system (two entries per event), for (c) partons within the same baryon and (d) for partons in opposite baryons. The data and prediction are as in (a).

balancing pairs based on minimum S . Four x 's were evaluated, since two partons contribute to each of the two pairs (see Fig. 1). Distributions of x are plotted in Figs. 20(a) and 20(b), along with a prediction obtained by applying the $\Delta S < 1.2$ selection to the admixture 90% MIXDP+10% PYTHIA. No systematic deviation of the DP rate vs x , and thus no x dependence to σ_{eff} , is apparent over the x range accessible to this analysis (0.01–0.40 for the photon+jet scattering, 0.002–0.20 for the dijet scattering).

Correlations in x between the partons that produce the two scatterings were investigated by plotting dijet x vs photon + 1 jet x . The ‘‘hot core’’ model, for example, predicts a correlation in x between two partons within the same baryon. In Fig. 20(c) we plot an average dijet x as a function of photon + 1 jet x , for partons within the same baryon. The use of an average dijet x allows any correlations to be more clearly seen. Because DP events originate from the scattering of four partons, each event makes two entries into Fig. 20(c), one for the pair of partons from the proton, and one for the pair of partons from the antiproton. For completeness, a complimentary plot for partons in opposite baryons is shown in Fig. 20(d). The 90% MIXDP+10% PYTHIA predictions are also shown. No correlations in x are apparent in either plot.

C. A search for other kinematic correlations

Apart from correlations introduced by x -dependent parton densities, other kinematic correlations between the two scat-

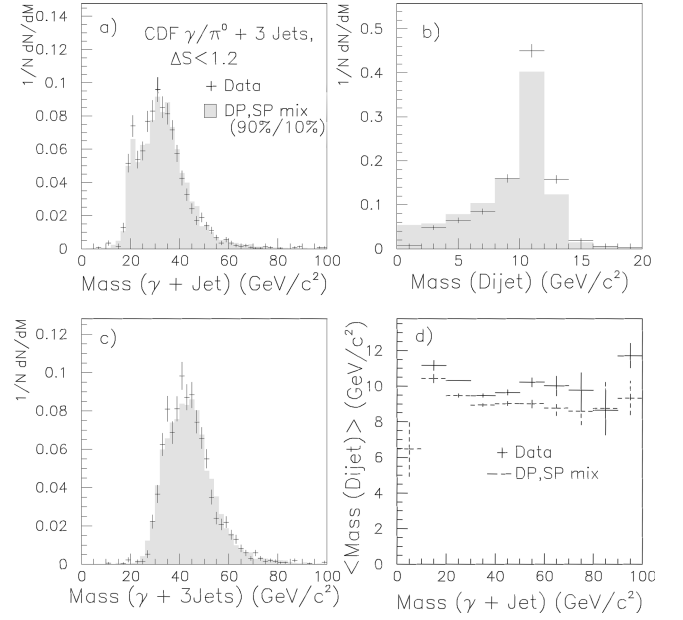


FIG. 21. Comparison of invariant mass for 1VTX data (points) and the mixture 90% MIXDP+10% PYTHIA (shaded). Events were required to have $\Delta S < 1.2$. (a) The photon+jet system. (b) The dijet system. (c) The four-body system. (d) Average dijet mass vs photon+jet mass. The data are well described by the prediction, which is dominated by the uncorrelated MIXDP model for DP.

terings could exist in DP events. Certainly for scatterings at high E_T , overall energy-momentum conservation restricts the x range available for the second scattering [27]. A second effect, more relevant for our relatively low E_T dataset, is that higher order processes contributing to DP might introduce a common transverse boost (‘‘ k_T kick’’) for the two pairs, as opposed to the independent boosts present in MIXDP.

We have searched for kinematic correlations using the DP-enriched data sample and prediction of Sec. IX B. Unlike the case of an x -dependent σ_{eff} , however, it is possible that some types of correlation would affect the distinguishing variable distributions, used in Sec. VI to establish the level of DP in the 1VTX sample. If such correlations are present, the MIXDP model is inadequate, and the value of f_{DP} and the purity of the enriched sample are uncertain. Any discrepancies seen between the properties of DP-enriched data and those of the 90% MIXDP+10% PYTHIA prediction could therefore reflect either (1) actual distortion of the enriched data due to DP correlations, or (2) an incorrect assumption for the purity of the enriched data.

The following variables were investigated: invariant mass, p_T , and longitudinal momentum p_z [28]. Each variable was evaluated for the two pairs separately and for the four-body system as a whole. The comparison of enriched data to the admixture 90% MIXDP+10% PYTHIA for these three kinematic variables is shown in Figs. 21–23. For example, Fig. 21 shows invariant mass distributions for both pairs, the four-body mass, and the average mass of the dijet pair as a function of the photon + 1 jet mass. This last is included to indicate the level of correlation between the pairs. The four-body and pairwise kinematic distributions are reasonably well described by the predicted mix of MIXDP and PYTHIA. At a detailed level, some differences are seen in the dijet p_T and mass. A low level of correlation is seen in both

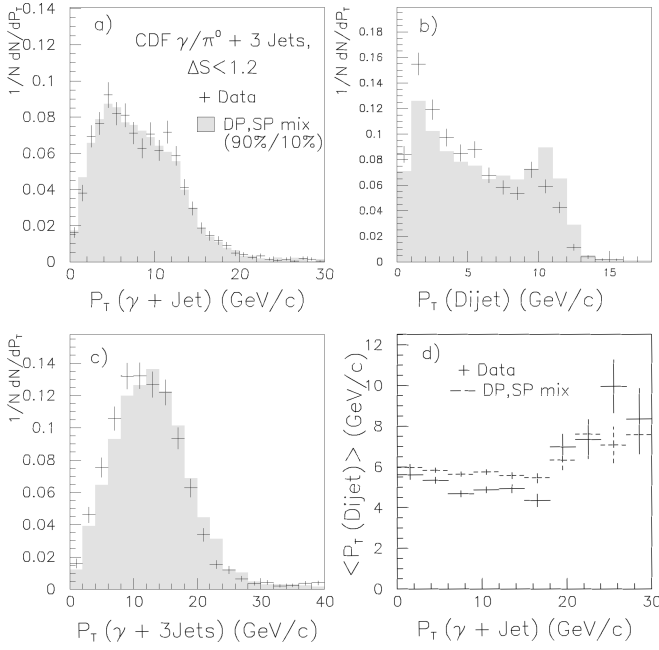


FIG. 22. Comparison of transverse momentum for 1VTX data (points) and the mixture 90% MIXDP+10% PYTHIA (shaded). See Fig. 21 for a description.

the data and prediction, and results from the fact that, according to MIXDP, the majority of DP events have the configuration shown in Fig. 2(c). For this event configuration the subdivision into photon + 1 jet and dijet systems is incorrect, and results in correlations between the two systems. The levels of correlation in DP-enhanced data are again reasonably well described by the prediction. We find no clear evidence of kinematic correlations in mass, p_T , or p_z .

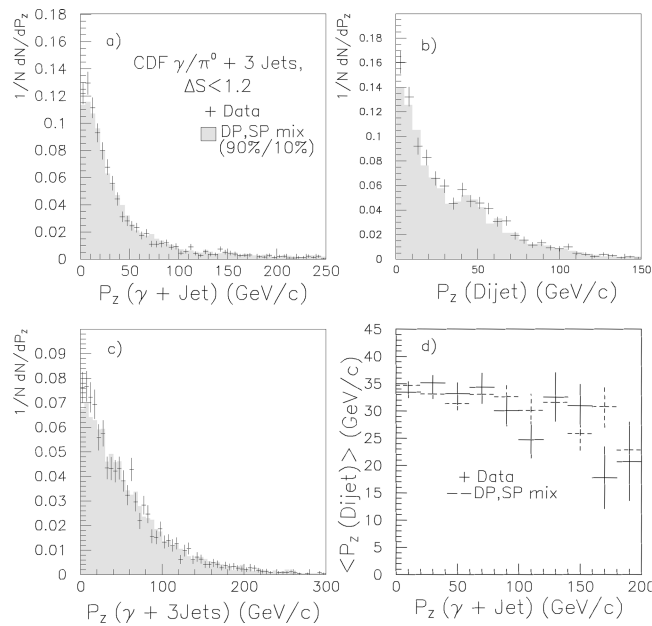


FIG. 23. Comparison of longitudinal momentum for 1VTX data (points) and the mixture 90% MIXDP+10% PYTHIA (shaded). See Fig. 21 for a description.

X. SUMMARY

A strong signal for the presence of double parton scattering has been observed in a sample of $\sim 14\,000$ CDF $\gamma/\pi^0 + 3$ jet events. We determine that the fraction of DP events in the sample is $(52.6 \pm 2.5 \pm 0.9)\%$, using a technique that does not rely on models for the single parton-parton scattering background processes. This represents nearly a factor of 10 increase in the ratio of DP to SP background, and a factor of 8 increase in the statistics of the DP candidate sample, over the previous CDF measurement. The process-independent parameter σ_{eff} is measured to be $(14.5 \pm 1.7^{+1.7}_{-2.3})$ mb, and was determined without reliance on theoretical QCD calculations. This measurement agrees well with the previous CDF value.

The σ_{eff} measurement has been used to constrain various models for the parton density distribution within the proton. Within the context of each of these models, σ_{eff} was used to evaluate a value of rms proton radius which was compared to measurements from ep elastic scattering experiments.

The high statistics and large DP signal fraction of this analysis have permitted searches for Feynman x dependence of σ_{eff} and kinematic correlations between the two hard scatterings. We find no evidence for x dependence to σ_{eff} within the x range of this analysis (0.01–0.40 for the $\gamma/\pi^0 + \text{jet}$ scatter, 0.002–0.20 for the dijet), and likewise no evidence for x correlations among the four partons involved in DP scattering. A search for kinematic correlations in mass, p_T , and p_z was also undertaken, and no correlations are observed.

ACKNOWLEDGMENTS

We wish to thank M. Drees, T. Han, and F. Halzen for useful discussions. We also thank the Fermilab staff and the technical staffs of the participating institutions for their vital contributions. This work was supported by the U.S. Department of Energy and National Science Foundation; the Italian Istituto Nazionale di Fisica Nucleare; the Ministry of Education, Science and Culture of Japan; the Natural Sciences and Engineering Research Council of Canada; the National Science Council of the Republic of China; the A. P. Sloan Foundation; and the Swiss National Science Foundation.

APPENDIX A: THE PROPERTIES OF CDF JETS WITH OBSERVED $E_T \sim 5$ GeV

In this appendix we investigate whether the low E_T jets of this analysis are the result of actual jet production, or of instrumental effects such as electronic noise, phototube discharge, or gas calorimeter sparking.

An inclusive 5 GeV jet data set was obtained from a sample of minimum bias trigger events. A total of 25 202 events were found with at least one jet above 5 GeV E_T and a single VTX vertex (9% of single vertex minimum bias events have one or more jets above 5 GeV). Of these, 706 events were flagged as resulting from obvious instrumental effects, with the jets originating with anomalously high rate from four specific calorimeter towers. We note that the remaining 24 496 events constitute the minimum bias ingredient events used in the creation of MIXDP events.

The strongest indicator of 5 GeV jets as being products of

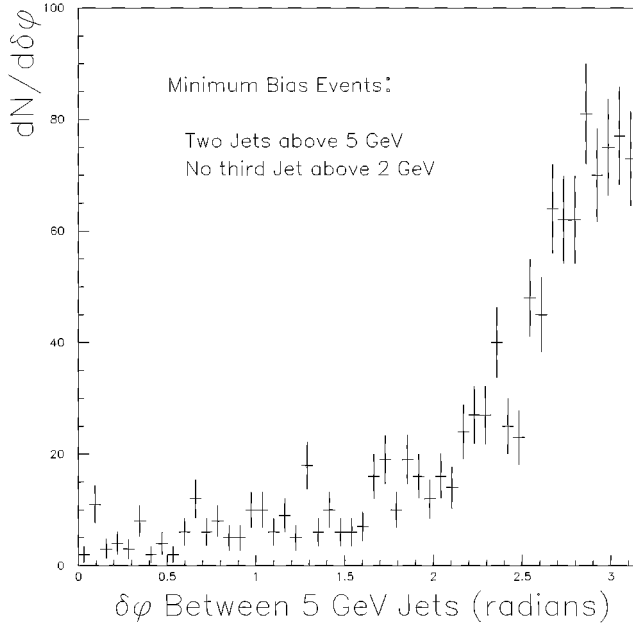


FIG. 24. Study of 5 GeV dijet events in minimum bias trigger data. The angle in ϕ between jets is plotted for a clean dijet sample, with both jets having $E_T > 5$ GeV and no others above 2 GeV.

hard scattering is the presence of dijet structure. If two 5 GeV jets in an event are approximately opposite one another in ϕ , then the jets are real and not the result of instrumental effects. In Fig. 24 we plot $\delta\phi$ in a sample of events with two jets, with both jets above 5 GeV and no third jet above 2 GeV. The third jets originate from either higher order QCD processes or DP scattering, and in either case tend to decorrelate the two leading jets. Strong correlation is seen in the 1119 events passing this tight selection.

Clearly, these observed two-jet events are real dijets, but this very clean data set represents only 5% of the inclusive 5 GeV jet sample. As a test of the remaining sample, the properties of inclusive 5 GeV jets and jets from the dijet sample were compared. The following comparisons are shown in Fig. 25: (a) the jet $|\eta|$ and (b) ϕ distributions, (c) the E_T spectra, (d) the ratio of the total momentum of CTC tracks within the jet cone to jet E_T (for jets with $|\eta| < 1$), (e) the ratio of EM calorimeter E_T to total E_T , and (f) average EM fraction vs jet $|\eta|$. The two data sets match well. The slight differences seen in some distributions are attributable to biases in the two samples, arising from the affect of E_T resolution coupled with the different requirements on the number of 5 GeV jets. By contrast, the properties of the 706 noise-produced jets are entirely different (CTC fraction < 0.1 , spikes in the EM fraction, etc.).

Apart from the explicit elimination of jets from four specific calorimeter regions we find no evidence for the contamination of 5 GeV jets by instrumental effects. Jets originating from noise in these regions were also eliminated from the $\gamma/\pi^0 + 3$ jet data samples and the event-mixing models of Sec. IV.

APPENDIX B: CORRECTION TO N_{DP} FOR TRIPLE PARTON SCATTERING

We use the MIXDP model to estimate the contamination of triple parton (TP) scattering events to the observed DP signal

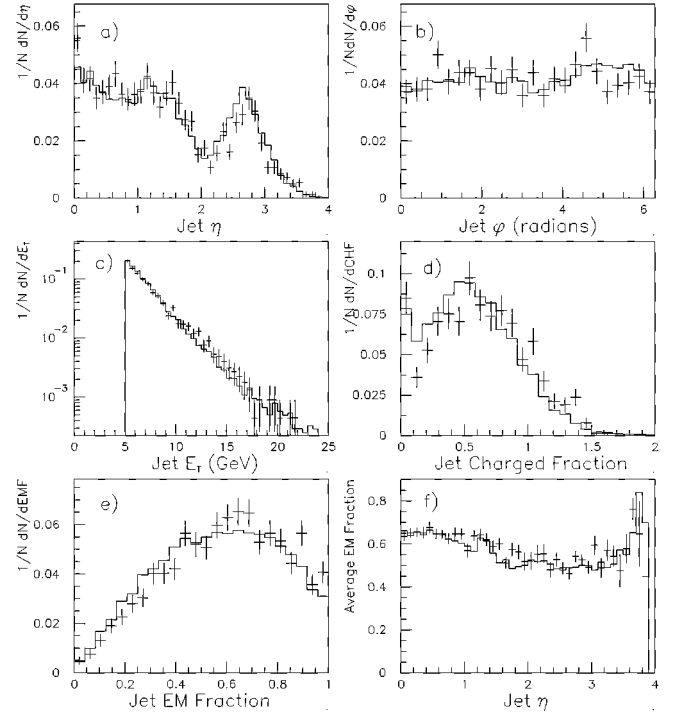


FIG. 25. Properties of inclusive 5 GeV jets in minimum bias trigger data (line) compared to jets from a clean dijet data set (points). The dijet distributions have entries for both jets. (a) Jet $|\eta|$, (b) ϕ , (c) E_T , (d) the ratio of total associated CTC track p_T to jet E_T , (e) the fraction of jet E_T seen in the EM calorimeter component, and (f) the average EM fraction vs jet $|\eta|$. Good matching is seen for the two data sets.

in data. For some fraction of MIXDP events, it is possible that a double parton scattering has occurred in one of the two ingredient events. The resulting MIXDP events model triple parton scattering.

The DP process can in principle occur in either of the two MIXDP ingredient events. Two combinations of ingredient events are possible which both yield a photon + 3 jets final state and include a double parton scattering in one of the ingredient events. These are shown in Figs. 4(c) and 4(d). In both cases, a total of two jets must fall below 5 GeV and thus be uncounted. The contribution of each of the two potential channels were evaluated separately.

The channel shown in Fig. 4(d) contributes to MIXDP events having the configuration (photon+2 jets)+(1 jet). To estimate the DP contribution to this channel, correlations within the photon + 2 jet ingredient event were studied. The angle in ϕ between the lowest E_T jet and the p_T vector of the remaining photon + 1 jet system was formed. This variable is similar to ΔS for photon + 3 jet events. The distribution of this variable was seen to have a flat tail extending to small angles, representing poor p_T balance, and was fit to a sum of predictions from SP (PYTHIA) and DP (event mixing used to produce photon + 2 jet events). We find that 30% of photon + 2 jet ingredient events are consistent with being DP. An upper limit on the DP contribution was obtained by assuming that all events at small $\delta\phi$ are DP, and extrapolating to all $\delta\phi$; this yields 38%. The lower limit is taken to be zero (i.e., no DP contribution to the photon + 2 jet MIXDP ingredient events) since higher order QCD processes, perhaps imper-

fectly modeled by PYTHIA, would also contribute to the poor-balance tail. Uncertainties are assigned such that these limits are reached at two standard deviations. Thus the DP contribution is $(30_{-15}^{+4})\%$ to MIXDP events using photon + 2 jet ingredient events. This configuration, (photon+2 jets)+(1 jet), comprises 72% of MIXDP events.

The second possible channel for DP contribution, Fig. 4(c), pertains to MIXDP events with the configuration (photon+1 jet)+(2 jets). Correlations in the two-jets ingredient event were studied. The ϕ angle between the two jets was plotted, and a tail extending to small angles was again seen. This flat tail when extended to all angles constitutes 43% of the events, and this value was taken to represent the maximum amount of double parton contribution to the two jet events. The minimum contribution was again taken to be 0, since higher order QCD processes would contribute to the small-angle tail. Taking the average of these values, and again defining uncertainties such that the limits are reached at two standard deviations, we find a DP contribution to the (photon+1 jet)+(2 jets) configuration of $(22 \pm 11)\%$. This configuration constitutes 28% of MIXDP events.

Combining the results for the two MIXDP configurations, we find $(28_{-14}^{+7})\%$ as the overall fraction of MIXDP events which use DP ingredient events. In principle, this should be the prediction for the TP contribution to the observed DP signal in 1VTX data. However, the assumption that the number of parton-parton scatterings per $\bar{p}p$ collision is distributed in a Poisson fashion [6] indicates that the prediction for the (photon+2 jets)+(1 jet) configuration is too large by a factor of 2. This results from the character of event mixing. In event mixing, the total number of independent hard scatterings in a mixed event is the sum of number of independent scatterings in the ingredient events. For example, when a SP photon + 2 jet ingredient event is combined with a SP 1 jet ingredient event, the resulting MIXDP event models DP. In the same way, the combination of a DP photon + 2 jet event and a SP 1 jet event yields a MIXDP event that models the TP process. Thus in event mixing the ratio of double to single scatters in photon + 2 jet ingredient events is equal to the ratio of triple to double scatters in the corresponding MIXDP events. On the other hand, under the Poisson assumption the ratio of triple to double scatters should be suppressed by *one-half* relative to the ratio of double to single scatters. This suppression is absent from event mixing. We therefore reduce the predicted fraction of DP in photon + 2 jets ingredient events from $(30_{-15}^{+4})\%$ to $(15_{-8}^{+2})\%$. No such reduction of the prediction is necessary for the (photon+1 jet)+(2 jets) configuration. The TP contribution to all MIXDP events is then $17_{-8}^{+4}\%$, and the corresponding correction factor for N_{DP} is $0.83_{-0.04}^{+0.08}$.

APPENDIX C: MODIFICATIONS TO THE σ_{eff} EXPRESSION

In this appendix we discuss modifications to the expression for determining σ_{eff} [Eq. (6)] resulting from event acceptance and vertex-finding efficiency, and assign an uncertainty to the vertex-related factor in the updated σ_{eff} expression. Additionally, we examine whether the two scatterings in our DP events in data are distinguishable or indistinguishable.

1. A special case: Constant instantaneous luminosity

As an aside, we first note an interesting simplification of Eq. 6 under special circumstances. The $N_c(1)/[2N_c(2)]$ factor in Eq. (6) is present because, to first order, DI events occur in beam crossings with two $\bar{p}p$ collisions while DP events occur in single-collision crossings. To gain insight into this factor, we note that if the instantaneous Tevatron luminosity were constant then $N_c(1)/[2N_c(2)] = \langle n \rangle^{-1}$, where $\langle n \rangle$ is the mean number of NSD collisions per beam crossing. This follows directly from the fact that the number of collisions per crossing has a Poisson distribution with mean $\langle n \rangle$. For this special case Eq. (6) reduces to a simple form:

$$\begin{aligned} \sigma_{\text{eff}} &= \left(\frac{N_{\text{DI}}}{N_{\text{DP}}} \right) \left(\frac{N_c(1)}{2N_c(2)} \right) \sigma_{\text{NSD}} = \left(\frac{N_{\text{DI}}}{N_{\text{DP}}} \right) \left(\frac{1}{\langle n \rangle} \right) \sigma_{\text{NSD}} \\ &= \left(\frac{N_{\text{DI}}}{N_{\text{DP}}} \right) \left(\frac{f_0}{\mathcal{L}_{\text{inst}}} \right). \end{aligned} \quad (\text{C1})$$

In the last step we used the relation $\langle n \rangle = (\mathcal{L}_{\text{inst}}/f_0)(\sigma_{\text{NSD}})$, with $\mathcal{L}_{\text{inst}}$ the instantaneous luminosity and f_0 the frequency of beam crossings. Thus, in this special case σ_{eff} is a simple function of the number of DP and DI events and two accelerator parameters.

2. Acceptance and vertex finding inefficiency

Returning to the general case of nonconstant instantaneous luminosity, we introduce the affects of event acceptance and vertex-finding efficiencies into Eq. (3), the expression for the expected number of DI events, and obtain

$$N_{\text{DI}} = A_{\text{DI}} \left(\frac{\sigma_{\gamma/\pi^0}}{\sigma_{\text{NSD}}} \right) \left(\frac{\sigma_J}{\sigma_{\text{NSD}}} \right) \sum_{n=2}^{\infty} n(n-1) N_c(n) \epsilon_2(n). \quad (\text{C2})$$

A_{DI} is the kinematic acceptance for DI events to pass the event selection, apart from the vertex requirement. The sum is over the number of collisions per beam crossing; at least two collisions are required for the DI process. The combinatorial factor of 2 in Eq. (3) generalizes to $n(n-1)$, n collisions taken two at a time. $N_c(n)$ is the number of beam crossings with n collisions. $\epsilon_2(n)$ is the efficiency for a DI event with n collisions to satisfy the 2VTX vertex requirements.

Similarly, Eq. (5), the expression for the expected number of DP events, becomes

$$N_{\text{DP}} = A_{\text{DP}} \left(\frac{\sigma_{\gamma/\pi^0} \sigma_J}{\sigma_{\text{eff}} \sigma_{\text{NSD}}} \right) \sum_{n=1}^{\infty} n N_c(n) \epsilon_1(n), \quad (\text{C3})$$

where A_{DP} is the kinematic acceptance for DP, the n factor is combinatorial (n collisions taken 1 at a time), and $\epsilon_1(n)$ is the efficiency for an n -collision DP event to pass the 1VTX vertex requirements. The sum over the number of collisions begins at 1. Taking the ratio of Eqs. (C2) and (C3), the updated expression for σ_{eff} is

$$\sigma_{\text{eff}} = \left(\frac{N_{\text{DI}}}{N_{\text{DP}}} \right) \left(\frac{A_{\text{DP}}}{A_{\text{DI}}} \right) (R_c) (\sigma_{\text{NSD}}), \quad (\text{C4})$$

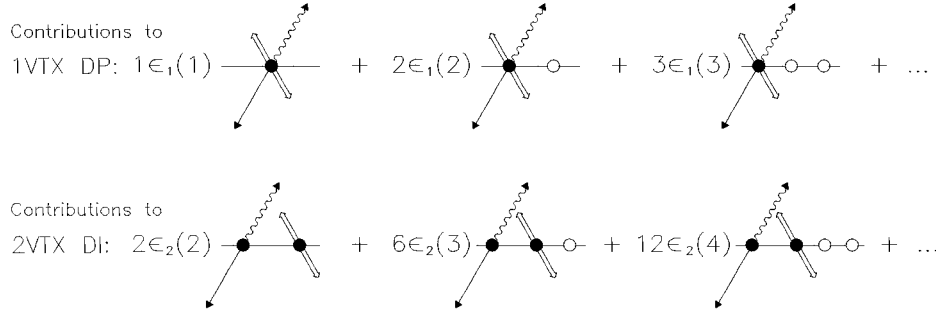


FIG. 26. Schematic representation of the sums over the number of $\bar{p}p$ collisions per beam crossing in Eqs. (C3) and (C2). Collisions found as VTX vertices are shown as solid circles, with unseen collisions shown as open circles. For example, a number of configurations contribute to the 1VTX DP sample. Single $\bar{p}p$ collision beam crossings contribute, scaled by the efficiency for finding the collision as a VTX vertex [$\epsilon_1(1)$]. Two collision crossings also contribute, scaled by a combinatorial factor of 2, since the scatter can be at either collision, and by the efficiency for finding one and only one of the collisions as a VTX vertex [$\epsilon_1(2)$], etc. Similarly for 2VTX DI events, where terms are scaled by larger combinatorial factors and the efficiency for finding 2 and only 2 VTX vertices in each configuration [$\epsilon_2(2)$, $\epsilon_2(3)$, etc.]. The efficiencies include the combinatorics of which collision(s) is found in each configuration.

where

$$R_c \equiv \frac{\sum_{n=1}^{\infty} n N_c(n) \epsilon_1(n)}{\sum_{n=2}^{\infty} n(n-1) N_c(n) \epsilon_2(n)}. \quad (\text{C5})$$

3. R_c and its uncertainty

The R_c factor results from the vertex requirements made to segregate the data into DP and DI candidate samples. The sum in the numerator (denominator) represents contributions to the 1VTX (2VTX) data set from crossings with n NSD collisions. These contributions are modulated by VTX vertex identification efficiencies. This is shown pictorially in Fig. 26. These inefficiencies arise both from detector and algorithmic inefficiencies, and the merging of close collisions into a single observed vertex.

VTX efficiencies were estimated in data. The overall efficiency for a DP scattering in an n -collision beam crossing to be found with 1 VTX vertex is $\epsilon_1(n)$, and was constructed from measured VTX efficiencies. The term for $n=1$ is 92%. The term for $n=2$ applies to events having a DP scattering and an accompanying NSD collision, where one collision is observed and the other lost; this is 22%. Other terms are negligible. Similarly, $\epsilon_2(n)$ is the overall efficiency for a DI event with n collisions to be found as 2VTX. The first non-zero term, $\epsilon_2(2)$, is 83%. The next term, $\epsilon_2(3)$, in which one of three collisions is unseen, is 20%.

Predictions for $N_c(n)$ are given in Sec. VIII. Combining these with $\epsilon_1(n)$ and $\epsilon_2(n)$, we find $R_c = 2.064 \pm 0.024$, where the uncertainty is statistical. If only the first term in each series is considered, meaning that only single collision beam crossings are taken to contribute to DP and double collisions to DI, then $R_c = 2.09$, showing that the leading terms dominate.

We now assign an uncertainty to R_c . This parameter depends on the number of NSD $\bar{p}p$ collisions per beam crossing and VTX reconstruction efficiencies. If our understanding of these issues is correct, a prediction can be made for the number of observed VTX vertices in any sample of CDF

data. The R_c expression [Eq. (C5)] is nearly identical to the expression for the ratio of the number of single to double VTX vertex events in any CDF hard-scattering sample:

$$\frac{\text{single VTX}}{\text{double VTX}} = \frac{\sum_{n=1}^{\infty} n N_c(n) \epsilon'_1(n)}{\sum_{n=2}^{\infty} n N_c(n) \epsilon'_2(n)}. \quad (\text{C6})$$

As a specific case, the inclusive photon trigger data set was chosen.

Vertex finding efficiencies in the VTX were found to be process dependent. As a result the efficiencies in Eq. (C6) differ from those in Eq. (C5). For example, consider the efficiency for two collision beam crossings to contribute to an event sample with two VTX vertices. In Eq. (C5) this is $\epsilon_2(2)$, and applies to DI events which have hard scatterings at both collisions. By contrast, $\epsilon'_2(2)$ in Eq. (C6) applies to inclusive photon events, which predominantly do not have a hard scattering at the second collision. The numerical values of the efficiencies are different [$\epsilon'_2(2) = 0.44$ compared to $\epsilon_2(2) = 0.83$, for this example], but the dominant first terms in the ratio of sums have the same form in Eqs. (C5) and (C6).

The measured ratio of single VTX vertex to double VTX vertex events in inclusive photon data is $4.96 \pm 0.02^{+0}_{-0.3}$, where systematic uncertainty arises from a subtraction of beam-gas background to the double VTX vertex data (i.e., events with one hard scattering vertex and one beam-gas vertex). Equation (C6) also yields 4.96. Because of the formal similarity in their expressions, we use the level of agreement between Eq. (C6) and the corresponding measurement as systematic uncertainty on R_c . The ratio of measurement to prediction is $1.000^{+0.005}_{-0.064}$, where statistical and systematic uncertainties on the measurement have been taken in quadrature. Applying this as systematic uncertainty on R_c , we obtain $R_c = 2.06 \pm 0.02^{+0.01}_{-0.13}$.

As a further check of the understanding of vertex related issues, the more demanding calculation of the ratio of the numbers of 3 VTX vertex events to single VTX vertex

events was also evaluated, and compared to a measurement made in the inclusive photon data. The ratio is 46.6 ± 0.5 in data, and the calculated value is 44.4. While not consistent with the data result within uncertainties, the calculation of this more complicated ratio is good to 5%.

4. Distinguishability: The m factor

In the derivations of Eqs. (6) and (C4) for σ_{eff} , it was stated that the cross sections for the individual scatterings cancel in the ratio of N_{DI} to N_{DP} . The question we address now is whether this cancellation is strictly true.

In Eq. (1) the m factor is 2 for DP final states consisting of two distinguishable scatterings. Indistinguishable scatterings have $m = 1$. For the $\gamma + 3$ jet final state in DP scattering the two constituent scatterings are clearly distinguishable. On the other hand, the $\pi^0 + 3$ jet process arises from a pair of scatterings which each results in a dijet. For the latter final state, it is possible that the scatterings are distinguishable because of the “asymmetric” kinematic cuts we impose, which insist that one scattering be “hard” (resulting in a $E_T \geq 16$ GeV π^0 and a jet) and that the accompanying scatter be “soft” (resulting in a dijet with two 5–7 GeV jets). This would argue for a factor of 2 for the $\pi^0 + 3$ jet final state.

This question was answered empirically. We first expand Eq. (1) to explicitly show the two processes:

$$\sigma_{\text{DP}} = \frac{2\sigma_\gamma\sigma_J + (m)\sigma_{\pi^0}\sigma_J}{2\sigma_{\text{eff}}}. \quad (\text{C7})$$

In analogy with the derivations in Sec. II, we write σ_γ symbolically as the cross section for $\gamma + 1$ or 2 jets production, and σ_J as production of 1 or 2 jets, such that taken together they yield a $\gamma + 3$ jet final state. Similarly, σ_{π^0} symbolically refers to 2 or 3 jet production including an energetic π^0 from jet fragmentation.

It is clear that the m factor affects the relative weighting of true photon events to π^0 events in the DP process. We determine m by comparing the fraction of true photons in

MIXDP events to a DP-enriched sample of data. For MIXDP, the relative weighting of photons to π^0 's is equivalent to having $m = 2$ in Eq. (C7), since the two scatterings are from separate events. If $m = 2$ for the $\pi^0 + 3$ jet DP events in data, then the true photon fractions of data and MIXDP should agree; if $m = 1$, they should not.

To obtain the fraction of true photons in DP events in the data, we examined 1VTX events with $\Delta S < 1.2$. The rationale is that the small ΔS region is DP enriched. Based on Fig. 14(f) the data after this cut have $f_{\text{DP}} = 90\%$. A total of 2575 data events satisfy the $\Delta S < 1.2$ requirement.

Three methods were employed to measure the fraction of true photons in MIXDP and DP-enriched 1VTX data. The first two are standard CDF techniques [15] that make use of (1) transverse shower shape in the CES and (2) the number of conversions seen in the CPR. In both methods, events are weighted by the probability that the photon candidate is a true photon. Summed over all events, the total weight is the estimated number of true photons. The third method fits the distribution of calorimeter energy seen in a cone $\Delta R < 0.7$ around the photon candidate to a sum of distributions for true photons and π^0 's. Using these techniques the true photon fraction for DP-enriched data was determined to be $(14.9 \pm 1.5 \pm 1.8)\%$, including a small correction for the estimated SP background remaining after the ΔS cut. The uncertainties are statistical and systematic, respectively. After applying the same ΔS cut to MIXDP events, we find a true photon fraction of $(14.7 \pm 0.3 \pm 0.5)\%$.

Clearly, the two true photon fractions are consistent within uncertainties. A value of m can be extracted from the comparison of the two fractions, and we find $m = 1.97 \pm 0.24 \pm 0.29$. This measured value supports the view that the $\pi^0 + 3$ jet DP events in our data are composed of distinguishable scatterings. We therefore take $m = 2$ for this analysis, in the extraction of σ_{eff} . Alternatively, had $m = 1$ been true for $\pi^0 + 3$ jet DP events in data, we would have expected to measure a photon fraction of 22.6%, nearly twice the MIXDP value.

-
- [1] C. Goebel *et al.*, Phys. Rev. D **22**, 2789 (1980); B. Humpert *et al.*, Phys. Lett. **154B**, 211 (1985).
 - [2] L. Ametller *et al.*, Phys. Lett. **169B**, 289 (1986).
 - [3] AFS Collaboration, T. Akesson *et al.*, Z. Phys. C **34**, 163 (1987).
 - [4] UA2 Collaboration, J. Alitti *et al.*, Phys. Lett. B **268**, 145 (1991).
 - [5] CDF Collaboration, F. Abe *et al.*, Phys. Rev. D **47**, 4857 (1993).
 - [6] T. Sjöstrand, Fermilab Report No. FERMILAB-Pub-85/119-T 1985.
 - [7] M. Drees and T. Han, Phys. Rev. Lett. **77**, 4142 (1996).
 - [8] T. Sjöstrand and M. Van Zijl, Phys. Lett. B **188**, 149 (1987).
 - [9] CDF Collaboration, F. Abe *et al.*, Phys. Rev. D **50**, 5550 (1994).
 - [10] CDF Collaboration, F. Abe *et al.*, Phys. Rev. Lett. **79**, 584 (1997).
 - [11] S. Ellis, Z. Kunszt, and D. Soper, Phys. Rev. Lett. **64**, 2121 (1990). See also F. Aversa, P. Chiappetta, M. Greco, and P. Guillet, *ibid.* **65**, 401 (1990); W. T. Giele, E. W. N. Glover, and D. A. Kosower, Nucl. Phys. **B403**, 633 (1993), and references therein.
 - [12] J. Huston *et al.*, Phys. Rev. D **51**, 6139 (1995).
 - [13] CDF Collaboration, F. Abe *et al.*, Nucl. Instrum. Methods Phys. Res. A **267**, 272 (1988).
 - [14] CDF Collaboration, F. Abe *et al.*, Phys. Rev. Lett. **73**, 2662 (1994); **74**, 1891E (1995).
 - [15] CDF Collaboration, F. Abe *et al.*, Phys. Rev. D **48**, 2998 (1993).
 - [16] CDF Collaboration, F. Abe *et al.*, Phys. Rev. D **45**, 1448 (1992).
 - [17] In prior CDF publications, the lowest E_T jets are those of the top quark measurement: CDF Collaboration, F. Abe *et al.*, Phys. Rev. Lett. **50**, 2626 (1995). Jets were accepted down to 8 GeV in uncorrected E_T .
 - [18] For MIXDI mixing, the transverse energies in all calorimeter

towers were stored for each ingredient event. During event mixing, tower E_T 's from one ingredient event were allowed to overlap with the observed jets in the other. In this way, all MIXDI jets effectively include the underlying event E_T associated with two $\bar{p}p$ hard scatterings. Calorimeter towers from the minimum bias ingredient event were also allowed to overlap with the photon candidate from the photon ingredient event.

- [19] T. Sjöstrand, Comput. Phys. Commun. **82**, 74 (1994).
- [20] CDF Collaboration, F. Abe *et al.*, Phys. Rev. Lett. **68**, 1104 (1992).
- [21] A χ^2 comparison between the data and PYTHIA for the two most distinguishing distributions, Figs. 6(a) and 6(f), yields 332/26 DF and 536/58 DF (statistical uncertainties only).
- [22] This effect is also seen in the comparison of $E_T(2)$ spectra for 1VTX and 2VTX data. The 2VTX spectrum is softer, and 2VTX events have a larger “double scatter component” (DP+DI) than 1VTX events.
- [23] The value from the $\delta\phi(\gamma, \text{jet } 2)$ fit is low, $(20 \pm 15)\%$. Refitting this variable with the constraint that $f_{\text{DP}} = 52.6\%$ worsens

the χ^2 from 27.3 to 34.0 for 29 Df, but the level of agreement is visually indistinguishable from the original fit. We conclude that the $\delta\phi(\gamma, \text{jet } 2)$ variable is consistent with 52.6%, but has limited distinguishing power in this method.

- [24] There are approximately 30% as many 2VTX events as 1VTX events, and 17.7% of 2VTX are DI. Thus the fraction of DI events compared to 1VTX is $0.3 \times 0.177 = 0.054$. Based on studies of vertex inefficiency, 4% of DI events will be found with 1 vertex. Thus the fraction of DI events faking single vertex events, compared to 1VTX, is $0.054 \times (0.04) = 0.0022$. Expressed as a fraction of the number of DP events, it is $0.0022/0.526 = 0.0042$.
- [25] D. Brown, Ph.D. thesis, Harvard University, 1989.
- [26] R. Hofstadter, Rev. Mod. Phys. **28**, 214 (1956).
- [27] T. Sjöstrand and M. Van Zijl, Phys. Rev. D **36**, 2019 (1987).
- [28] The pairwise mass and p_z are functions of the Feynman x 's. For example, $M(\text{dijet}) \propto \sqrt{x_p^{JJ} x_{\bar{p}}^{JJ}}$, and $p_z(\text{dijet})$ is related to $x_p^{JJ} - x_{\bar{p}}^{JJ}$. These are combinations of the Feynman x 's not tested in the previous section.